ATTACHMENT 6

AREVA Document #32-9244434-002, "Byron and Braidwood RVCH Nozzle As-Left J-Groove Analysis"

NON-PROPRIETARY

AREVA

CALCULATION SUMMARY SHEET (CSS)

Document No. 32 - 9244434 - 002 Safety Related: ☒Yes ☐ No

Title Byron and Braidwood RVCH Nozzle As-Left J-Groove Analysis- Non Proprietary

PURPOSE AND SUMMARY OF RESULTS:

PURPOSE:

Due to concerns that Control Rod Drive Mechanism (CRDM), core exit thermocouple (CETC), and reactor vessel level indication system (RVLIS) nozzle penetration degradation may have occurred in the Reactor Vessel Closure Heads (RVCHs) at Byron Station, Units 1 and 2, and Braidwood Station, Units 1 and 2, Exelon Generation Company, LLC (Owner) contracted AREVA to create a modification to repair these nozzles as a contingency. In the event that a repair is necessary, an ID temper bead weld repair procedure has been developed wherein the lower portion of the nozzle is removed by a boring procedure and the remaining portion is welded to the low alloy steel reactor vessel head above the original Alloy 82/182 J-groove attachment weld. Per Reference [1], fracture mechanics analysis must be performed to justify the worst-case flaw(s) remaining in the original nozzle-to-RVCH weld (as-left J-groove weld) at the worst-case location(s)

The purpose of this calculation is to perform a fracture mechanics analysis of the worst-case flaws in the as-left J-groove weld at the worst-case penetration location. This analysis considers the worst-case nozzle location and utilizes material properties which bound the properties of all four units.

This document is the Non-Proprietary document for 32-9236713-003.
Proprietary information is contained within bold square brackets "[ ]".

SUMMARY OF RESULTS:

A fatigue crack growth and fracture mechanics evaluation of the worst-case flaws in the as-left J-groove weld and buttering at the worst-case penetration location has been performed. Based on a combination of linear elastic and elastic-plastic fracture mechanics the postulated flaws are shown to be acceptable for the remaining life utilizing the safety factors in Table 1-1, and the lower bound J-R Curve from Regulatory Guide 1.161.

Limitation: The minimum metal temperature for performing a Hydrostatic test at any time after an IDTB repair has been made is **[ ]**

The following table summarizes the total pages contained in this document.

Section	Main Body	Appendix A	Appendix B	Appendix C	Total
Pages	60	23	23	5	111

If the computer software used herein is not the latest version per the EASI list, AP 0402-01 requires that justification be provided.

THE FOLLOWING COMPUTER CODES HAVE BEEN USED IN THIS DOCUMENT:

CODE/VERSION/REV	CODE/VERSION/REV
ANSYS 14.5.7 *	
*See Section 5.1 for justification.	

THE DOCUMENT CONTAINS ASSUMPTIONS THAT SHALL BE VERIFIED PRIOR TO USE

☐Yes

☒ No

AREVA

Byron and Braidwood RVCH Nozzle As-Left J-Groove Analysis- Non Proprietary

Review Method: ☒ Design Review (Detailed Check)

☐ Alternate Calculation

Signature Block

Name and Title (printed or typed)	Signature	P/R/A and LP/LR	Date	Pages/Sections Prepared/Reviewed/Approved
Silvester Noronha Principal Engineer		P	11/1/16	All
Tom Riordan Engineer IV		R	01NOV2016	All
Tim Wiger Engineering Manager		A	11/1/16	All

Notes: P/R/A designates Preparer (P), Reviewer (R), Approver (A);
LP/LR designates Lead Preparer (LP), Lead Reviewer (LR)

In reviewing and approving the initial release (Rev. 000), the lead reviewer/approver shall designate 'All' in pages/sections reviewed/approved.

In reviewing and approving revisions, the lead preparer and lead reviewer shall use 'All' in the pages/sections reviewed/approved. 'All' means that the changes and the effect of the changes on the entire document have been reviewed/approved. It does not mean that the lead reviewer/approver has reviewed/approved all the pages of the document.

Project Manager Approval of Customer References (N/A if not applicable)

Name (printed or typed)	Title (printed or typed)	Signature	Date
N/A			

Signature Block
(Continued)

Mentoring Information (not required per 0402-01)

Name (printed or typed)	Title (printed or typed)	Mentor to: (P/R)	Signature	Date
N/A				

Record of Revision

Revision No.	Pages/Sections/Paragraphs Changed	Brief Description / Change Authorization
000	All	Initial Release
001	All	This is a complete Revision. Non-Proprietary document for 32-9236713-002
002	Section 4.2.1	Redacted proprietary material designations.
	Section 4.2.2	Redacted proprietary material designation and material property values in the tables.
		Non-Proprietary document for 32-9236713-003.

Table of Contents

Page

Table of Contents
(continued)

Page

List of Tables

List of Tables
(continued)

Page

List of Figures

1.0 PURPOSE

Due to concerns that Control Rod Drive Mechanism (CRDM), core exit thermocouple (CETC), and reactor vessel level indication system (RVLIS) nozzle penetration degradation may have occurred in the RVCHs at Byron Station, Units 1 and 2, and Braidwood Station, Units 1 and 2, Exelon Generation Company, LLC (Owner) contracted AREVA to create a modification to repair these nozzles as a contingency. In the event that a repair is necessary, an ID temper bead weld repair procedure has been developed wherein the lower portion of the nozzle is removed by a boring procedure and the remaining portion is welded to the low alloy steel reactor vessel head above the original Alloy 82/182 J-groove attachment weld. Per Reference [1], fracture mechanics analysis must be performed to justify the worst-case flaw(s) remaining in the original nozzle-to-RVCH weld (as-left J-groove weld) at the worst-case location(s). Since a potential flaw in the J-groove weld cannot be sized by currently available non-destructive examination techniques, it is considered that the worst-case as-left condition of the remaining J-groove weld includes degraded or cracked weld material extending through the entire J-groove weld and Alloy 82/182 butter material (due to PWSCC). It is further postulated that this flaw could propagate into the low alloy steel head by fatigue.

The purpose of this calculation is to perform a fracture mechanics analysis of the worst-case flaws in the as-left J-groove weld at the worst-case penetration location. This analysis considers the worst-case nozzle location and utilizes material properties which bound the properties of all four units.

Per Reference [1] the applicable code is ASME Section XI, 2001 Edition with Addenda through 2003 (Reference [2]) for Braidwood Units 1 and 2, and 2007 Edition with Addenda through 2008 for Byron Units 1 and 2 (Reference [28]). Analysis in this document utilizes Reference [2], which is more restrictive than Reference [28] (see Section 2.6). If the service life of the component is shown to be limited, an alternate approach of using ASME Section XI Code Case N-749 (Reference [3]) as modified by the Nuclear Regulatory Commission (see attachment to Reference [4]), which is more conservative than the most recent equation proposed by NRC in Reference [29], will be considered in the evaluation. Acceptance of each postulated flaw is determined based on available fracture toughness or ductile tearing resistance using the safety factors outlined in Table 1-1.

The purpose of revision 002 is to address the [ ] (Appendix C).

Table 1-1: Safety Factors for Flaw Acceptance

LEFM*			
Operating Condition	Evaluation Method	Fracture Toughness / K_I	
Normal/Upset	K_{Ia} fracture toughness	$\sqrt{10} = 3.16$	
Emergency/Faulted	K_{Ic} fracture toughness	$\sqrt{2} = 1.41$	
EPFM Based on Limited Ductile Flaw Extension**			
Operating Condition	Evaluation Method	Primary	Secondary
Normal/Upset	$J_{0.1}$ limited flaw extension	2.0	1.0
Emergency/Faulted	$J_{0.1}$ limited flaw extension	1.5	1.0
EPFM Based on Limited Ductile Flaw Extension and Stability***			
Operating Condition	Evaluation Method	Primary	Secondary
Normal/Upset	J/T based flaw stability	2.14	1.0
Normal/Upset	$J_{0.1}$ limited flaw extension	1.5	1.0
Emergency/Faulted	J/T based flaw stability	1.2	1.0
Emergency/Faulted	$J_{0.1}$ limited flaw extension	1.25	1.0

*LEFM safety factors are from IWB-3612 of ASME Section XI (Reference [2]).
**EPFM safety factors based on Section 3.1 of Code Case N-749 (Reference [3]).
***EPFM safety factors based on Section 3.2 of Code Case N-749 (Reference [3]).

2.0 ANALYTICAL METHODOLOGY

The basic analytical methodology is outlined below. Details are provided in the following subsections.

1. Postulate radial-axial flaws in the J-groove weld and butter of the worst case nozzle location. Past experience has shown that the nozzle with the largest hillside angle is the worst case location, which for the current configuration is the CETC nozzle. The radial-axial flaws are postulated since the hoop stresses are dominant.
2. Develop explicit three dimensional finite element crack models of the postulated flaws on the uphill and downhill side in order to calculate the stress intensity factors (SIFs). In order to determine SIFs at varying flaw sizes two uphill crack models and two downhill crack models will be generated with increasing flaw sizes.
3. Develop a mapping procedure to transfer stresses from an uncracked finite element stress model to the crack face of each crack model, enabling stress intensity factors to be calculated for arbitrary stress distributions over the crack face utilizing the principle of superposition. This strategy makes it possible to obtain pressure and thermal stresses from independent thermal/structural analyses and transfer these stresses to the crack model to support flaw evaluation. Mapping is used for the present assignment to apply residual stresses from weld residual stress analysis and operating stresses from Section III fatigue analysis to the three-dimensional crack models discussed above.
4. Obtain stress intensity factors for each loading condition at varying positions along the crack front by using the ANSYS KCALC command.
5. Calculate fatigue crack growth for cyclic loading conditions using operational stresses from pressure and thermal loads and crack growth rates from Article A-4300 of Section XI for ferritic material in a primary water environment. Residual stresses are included in the fatigue crack growth calculations as a mean stress, which affects the fatigue crack growth rates through the R ratio (K_{min}/K_{max}).
6. Utilize the screening criteria of ASME Code Case N-749 (Reference [3]) as modified by the NRC (Reference [4]) to determine the appropriate method of analysis (LEFM or EPFM). For LEFM flaw evaluations, compare the stress intensity factors to the available fracture toughness, with appropriate safety factors. When the material is more ductile and EPFM is the appropriate analysis method, evaluate in accordance with ASME Code Case N-749 (Reference [3]). A limit load analysis is performed to demonstrate that Items 3.1(c) or 3.2(a)(3) of Reference [3] are satisfied. Items 3.1(c) or 3.2(a)(3) requires that the primary stress limit of NB-3000 are satisfied, considering a local reduction of the pressure boundary area equal to the area of the flawed material.

2.1 Stress Intensity Factor Solution

The SIF solutions for the postulated flaws evaluated by fracture mechanics analysis are calculated using three-dimensional finite element models with crack tip elements. The model includes the Reactor Vessel Closure Head (RVCH) with existing J-groove weld. The nozzle and IDTB weld are conservatively not included since these materials would provide additional constraint, limiting the crack opening. An isometric view of the overall finite element model developed for this analysis is shown in Figure 2-1.

Radial-axial flaws are postulated and analyzed separately on the uphill and downhill sides of the nozzle and shown in Figure 2-2 and Figure 2-3. For each postulated flaw two finite element models are generated with a flaw size increment of 0.625" in order to capture the variation of SIF with flaw size. For each postulated flaw, SIFs are calculated at a total of 17 positions along the crack front starting with position 1 at the RVCH ID and going to position 17 at the nozzle bore as shown in Figure 2-2 and Figure 2-3. Stress intensity factors are

calculated using the ANSYS KCALC command (Reference [23]), which determines the stress intensity factors based on displacements in the vicinity of the crack tip. For "non-classical" flaw shapes with stress intensity factor calculated by the finite element method it is both difficult and unnecessary to prescribe an initial flaw size. In order to track the flaw size during fatigue crack growth any characteristic dimension may be used as the initial flaw size. For this calculation the initial flaw size, a_0, is chosen to be the vertical distance along the penetration bore in the finite element model from the inside surface of the cladding to the butter/head interface (see Figure 2-4).

Stress intensity factors at flaw sizes between the modeled flaw sizes are linearly interpolated. If the flaw size is larger than the largest flaw in the finite element model, the stress intensity factor is determined using the following scaling rule

$$K_I(a_2) = K_I(a_1)\sqrt{\frac{a_2}{a_1}}$$

where $K_I(a_1)$ is a known SIF at flaw size a_1 and $K_I(a_2)$ is the desired SIF at flaw size a_2. This approach follows from the fundamental expression for the stress intensity factor, $K_I = \sigma\sqrt{\pi a}$, where for a given applied stress and geometry the stress intensity factor scales with the square root of flaw size.

2.1.1 Plastic Zone Correction

The Irwin plastic zone correction is used to account for a moderate amount of yielding. For plane strain conditions the correction is (Reference [5], Eq. 2.63)

$$r_y = \frac{1}{6\pi}\left(\frac{K_I(a)}{\sigma_y}\right)^2$$

where $K_I(a)$ is the stress intensity factor at the actual crack size (a), and σ_y is the material's yield strength. The effective crack size, a_e, is calculated as

$$a_e = a + r_y$$

The stress intensity factor at the effective flaw size is then calculated using the scaling law derived above as

$$K_I(a_e) = K_I(a)\sqrt{\frac{a_e}{a}}$$

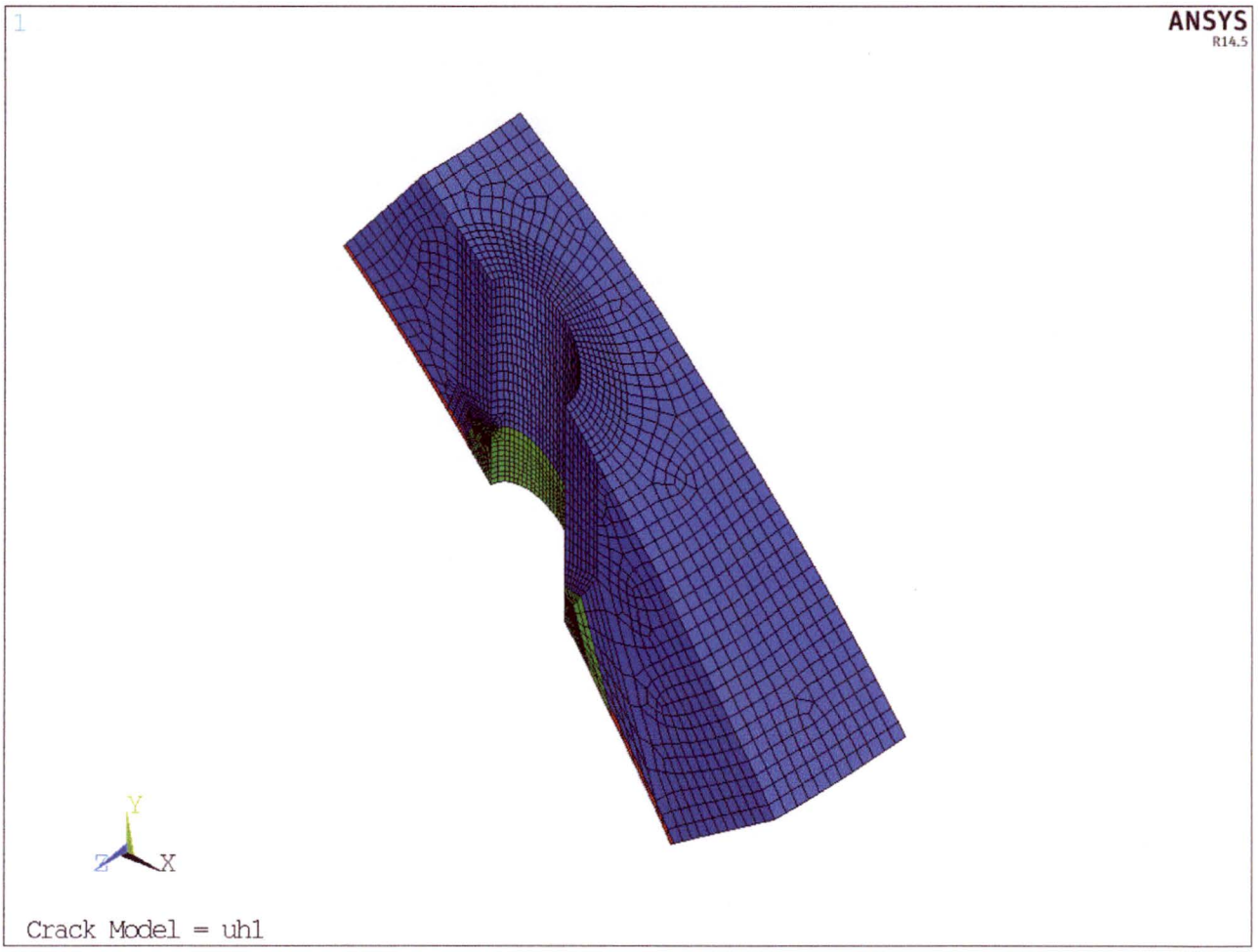

Figure 2-1: Finite Element Model Isometric View

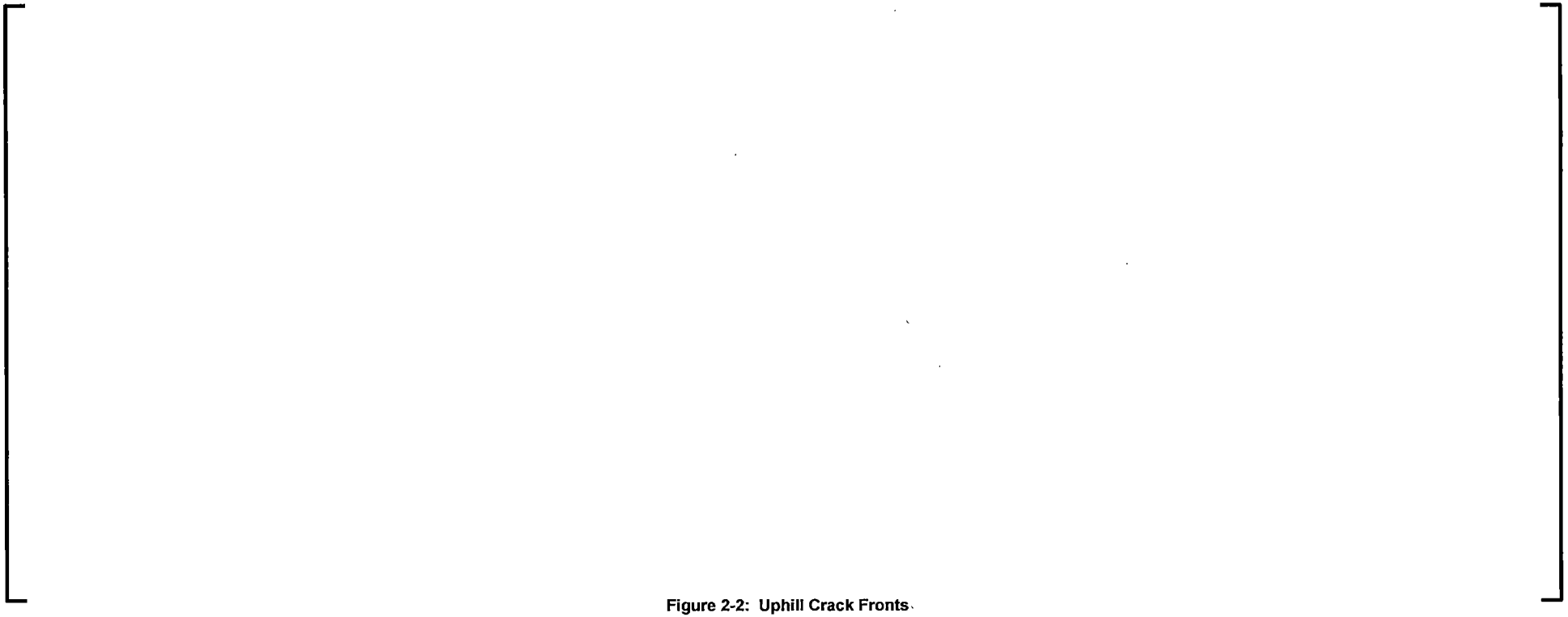

Figure 2-2: Uphill Crack Fronts

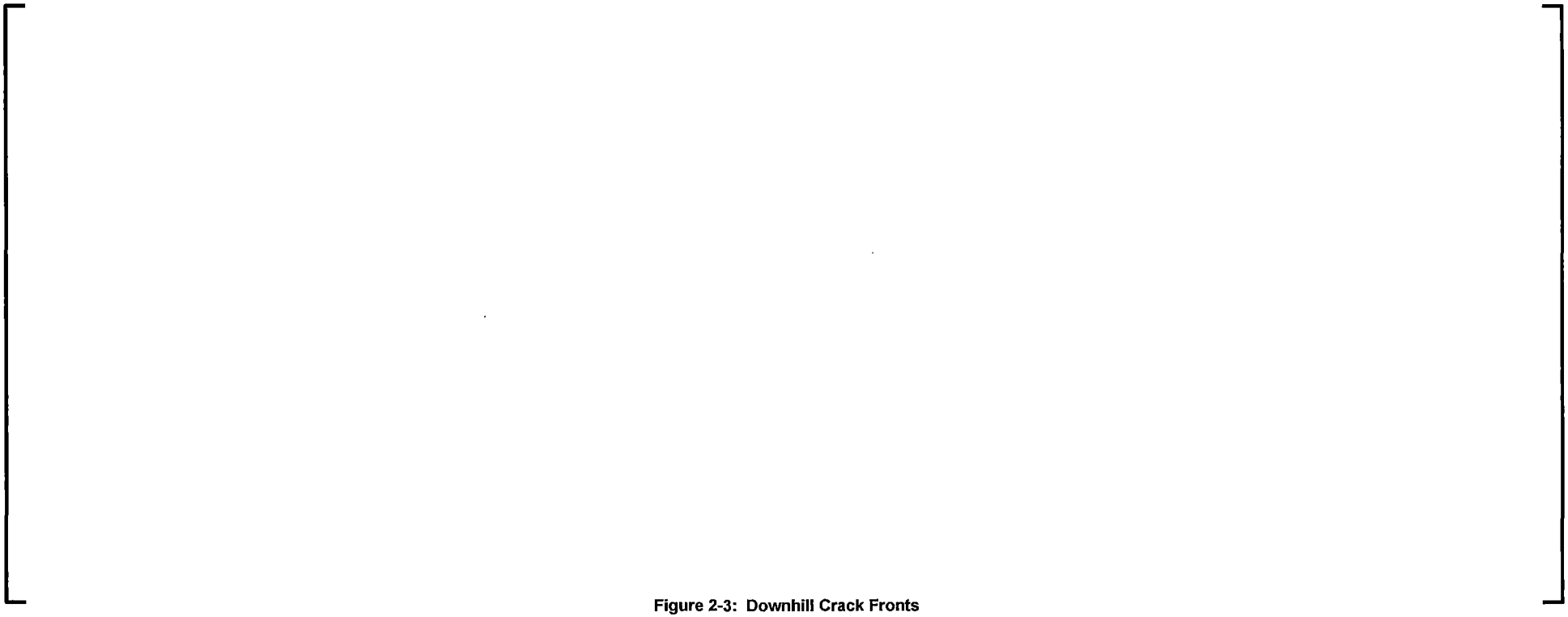

Figure 2-3: Downhill Crack Fronts

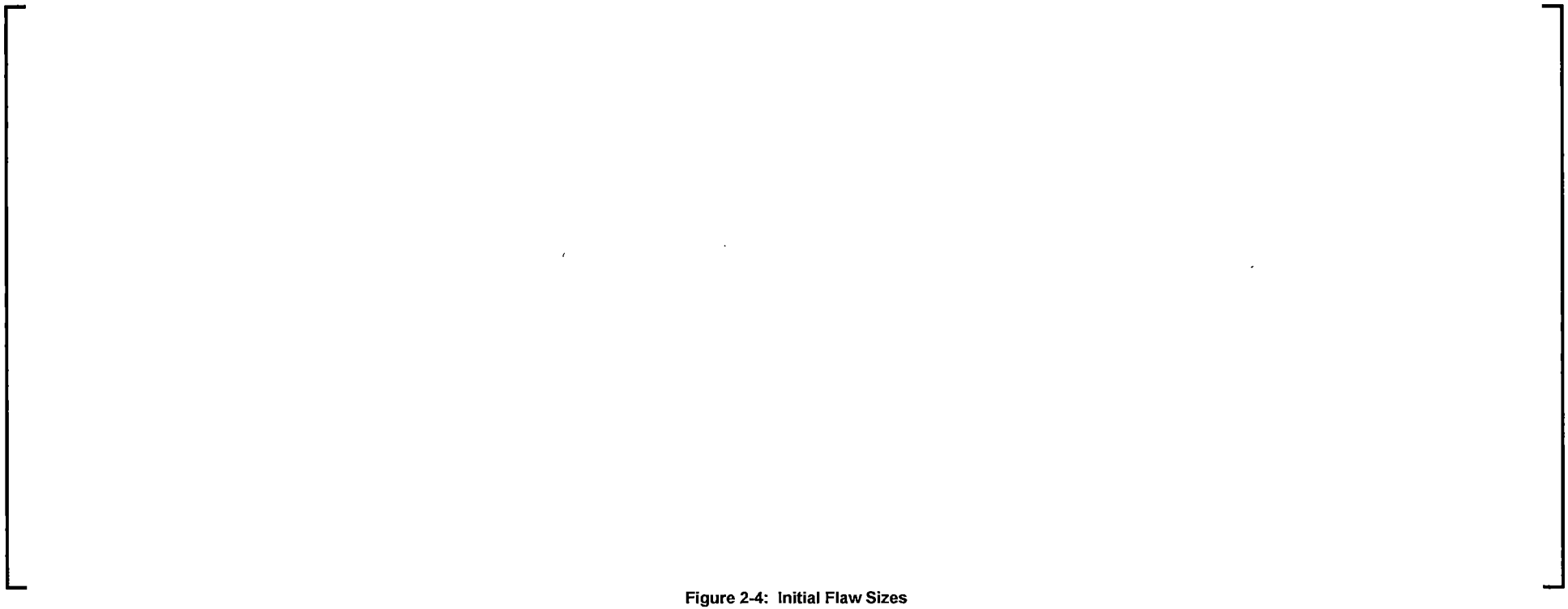

Figure 2-4: Initial Flaw Sizes

2.2 Fatigue Crack Growth

Fatigue crack growth is calculated using the fatigue crack growth rate model from Article A-4300 of Reference [2] as

$$\frac{da}{dN} = C_0(\Delta K_I)^n$$

where ΔK_I is the stress intensity factor range in ksi$\sqrt{in}$, and da/dN is the crack growth rate in inches/cycle. The crack growth rates for a surface flaw will be utilized since the postulated flaw(s) would result in the low alloy steel head being exposed to the primary water environment.

The detailed equations for calculating the fatigue crack growth rate are presented below.

$$\Delta K_I = K_{Max} - K_{Min}$$

$$R = K_{Min}/K_{Max}$$

$0 \le R \le 0.25$, $\Delta K_I < 17.74$

$$n = 5.95$$
$$S = 1.0$$
$$C_0 = 1.02 \times 10^{-12} S$$

$\Delta K_I \ge 17.74$

$$n = 1.95$$
$$S = 1.0$$
$$C_0 = 1.01 \times 10^{-7} S$$

$0.25 \le R \le 0.65$, $\Delta K_I < 17.74[(3.75R + 0.06)/(26.9R - 5.725)]^{0.25}$

$$n = 5.95$$
$$S = 26.9R - 5.725$$
$$C_0 = 1.02 \times 10^{-12} S$$

$\Delta K_I \ge 17.74[(3.75R + 0.06)/(26.9R - 5.725)]^{0.25}$

$$n = 1.95$$
$$S = 3.75R + 0.06$$
$$C_0 = 1.01 \times 10^{-7} S$$

$0.65 \le R \le 1.00$, $\Delta K_I < 12.04$

$$n = 5.95$$
$$S = 11.76$$
$$C_0 = 1.02 \times 10^{-12} S$$

$\Delta K_I \ge 12.04$

$$n = 1.95$$
$$S = 2.5$$
$$C_0 = 1.01 \times 10^{-7} S$$

2.3 Linear Elastic Fracture Mechanics

After fatigue crack growth is calculated the flaw is evaluated using Linear Elastic Fracture Mechanics (LEFM). Article IWB-3612 of Section XI (Reference [2]) requires that the applied stress intensity factor be less than the available fracture toughness at the crack tip temperature, with appropriate safety factor, as outlined below.

Normal/Upset Conditions: $K_I < K_{Ia}/\sqrt{10}$

Emergency/Faulted Conditions: $K_I < K_{Ic}/\sqrt{2}$

In the above K_{Ia} is the fracture toughness based on crack arrest and K_{Ic} is the fracture toughness based on crack initiation. In the evaluation of the above limits, a plastic zone correction is incorporated using the methodology described in Section 2.1.1.

2.4 Elastic-Plastic Fracture Mechanics

Elastic-plastic fracture mechanics (EPFM) will be used as an alternative acceptance criteria when the flaw related failure mechanism is unstable ductile tearing. LEFM would be used to assess the potential for non-ductile failure, while limit analysis would be used to check for plastic collapse.

2.4.1 Screening Criteria

ASME Code Case N-749 states that EPFM acceptance criteria are applicable to ferritic steel components on the upper shelf of the Charpy energy curve when the metal temperature exceeds the upper shelf transition temperature, T_c. The NRC has proposed a modification to the Code Case definition of T_c, which is given below (see Reference [4]).

$$T_c = 170.4°\text{F} + 0.814 \times RT_{NDT}$$

When the metal temperature exceeds T_c, EPFM analysis is applicable, otherwise LEFM analysis is applicable.

It is noted that more recently, the NRC has proposed a slightly different equation for T_c in Reference [29]. This more recently proposed equation is less restrictive (i.e., allows EPFM at lower temperature), and thus the equation above used in this analysis is conservative.

2.4.2 Flaw Stability and Crack Driving Force

Elastic-plastic fracture mechanics analysis will be performed based on ASME Code Case N-749 (Reference [3]) to evaluate crack driving force and flaw stability (if applicable). Two possible sets of acceptance criteria for EPFM are defined in Code Case N-749:

- Section 3.1 Acceptance Criteria Based Solely on Limited Ductile Crack Extension, or
- Section 3.2 Acceptance Criteria Based on Limited Ductile Crack Extension and Stability.

Section 3.1 states that the flaw is acceptable if the crack driving force, as measured by the applied J-integral (J_{app}) with appropriate safety factors applied to the loads, is less than the than the J-integral of the material (J_{mat}) at a ductile crack extension of 0.1 inch ($J_{0.1}$). If the criteria of Section 3.1 are not met, the flaw may still be acceptable if the criteria of Section 3.2 are met. Section 3.2 allows lower safety factors for the crack driving force check, and additionally requires that flaw stability be evaluated with appropriate safety factors. The flaw stability analysis will be performed using a J-integral/tearing modulus (J-T) diagram to evaluate flaw stability under ductile tearing, where J is either the applied (J_{app}) or the material (J_{mat}) J-integral, and T is the tearing modulus, defined as (E/σ_f^2) $(\partial J/\partial a)$. Flaw stability and crack driving force assessments will utilize the safety factors from Code Case N-749 as outlined in Table 1-1.

The general methodology for performing an EPFM analyses is outlined below.

Let $E'=$ $E/(1-\nu^2)$

Final flaw depth = a

Total applied $K_I=$ K_{Iapp}

K_I due to pressure (primary) = K_{Ip}

K_I due to residual plus thermal (secondary) = $K_{Is} = K_{Iapp} - K_{Ip}$

Safety factor on primary loads = SF_p

Safety factor on secondary loads = SF_s

Total applied K_I with safety factors, $K_I^*=$ $SF_p*K_{Ip} + SF_s*K_{Is}$

For small scale yielding at the crack tip, a plastic zone correction (see Section 2.1.1) is used to calculate an effective flaw depth based on

$$a_e = a + \frac{1}{6\pi}\left(\frac{K_I^*}{\sigma_y}\right)^2$$

which is used to update the total applied stress intensity factor based on

$$K_I' = K_I^*\sqrt{\frac{a_e}{a}}$$

The applied J-integral is then calculated using the relationship

$$J_{app} = {(K_I')^2}/{E'}$$

The applied J-integral is checked against $J_{0.1}$, demonstrating that the crack driving force falls below the J-R curve at a crack extension of 0.1 inch.

For flaw stability analysis, the final parameter needed to construct the J-T diagram is the tearing modulus. The applied tearing modulus, T_{app}, is calculated by numerical differentiation for small increments of crack size (da) about the crack size (a), according to

$$T_{app} = \frac{E}{\sigma_f^2}\left(\frac{J_{app}(a+da) - J_{app}(a-da)}{2\,da}\right)$$

The material J-T curve is determined as described in Section 4.2. Constructing the J-T diagram as shown below,

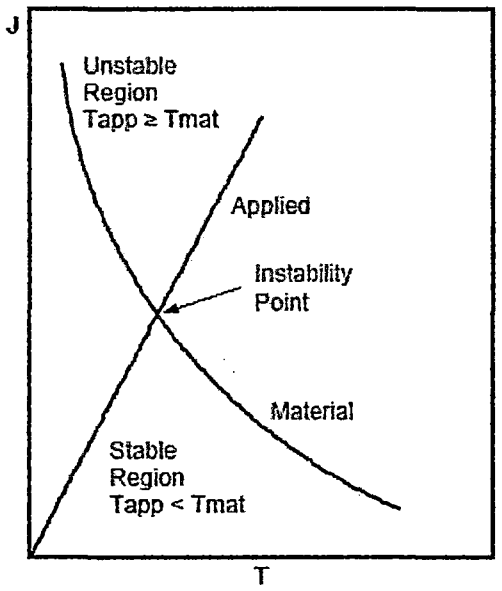

flaw stability is demonstrated at an applied J-integral when the applied tearing modulus is less than the material tearing modulus. Alternately, the applied J-integral is less than the J-integral at the point of instability.

2.5 Primary Stress Analysis

Items 3.1(c) and 3.2(a)(3) of Reference [3] state that the flawed component must meet the primary stress limits of NB-3000, assuming a local area reduction of the pressure retaining membrane that is equal to the area of the flaw. To evaluate the requirement, article NB-3228.1 of Section III of the ASME Code [24] is utilized. NB-3228.1 states that the limits on General Membrane Stress Intensity (NB-3221.1), Local Membrane Stress Intensity (NB-3221.2), and Primary Membrane Plus Primary Bending Stress Intensity (NB-3221.3) need not be satisfied at a specific location if it can be shown by limit analysis that the specified loadings do not exceed two-thirds of the lower bound collapse load. The yield strength to be used in these calculations is $1.5S_m$. Per NB-3112.1(a) the Design Pressure shall be used in showing compliance with this limit.

2.6 Section XI Code Year Reconciliation

The only applicable change in Section XI between the 2001 Edition with Addenda through 2003 (Reference [2]) and the 2007 Edition with Addenda through 2008 (Reference [28]) is in the IWB-3612(a) acceptance criteria for normal and upset conditions. IWB-3612(a) of Reference [28] allows the use of the K_{IC} measure of fracture toughness, while IWB-3612(a) of Reference [2] uses the more restrictive K_{Ia} and is conservatively bounding. Therefore, use of Reference [2] throughout this analysis is acceptable.

3.0 ASSUMPTIONS

3.1 Unverified Assumptions

No unverified assumptions are used in this calculation.

3.2 Justified Assumptions

The following justified assumptions are used in this calculation:

1. For fatigue crack growth calculations cycles are assumed to accumulate at a linear rate, i.e., in each year the number of cycles utilized is the total number of design cycles divided by the plant design life. This assumption is reasonable since experience shows that linear rates generally envelope the accumulation rates observed for transients based on plant operating experience (see Reference [6], TODI-BYR-15-008 cycle counts).
2. A 20 year license extension for each unit is assumed. Based on this and review of current license expiration dates for each unit fatigue crack growth for 33 years is considered.
3. For the limit load analysis (Section 6.5.1), an eighth symmetric model is utilized. The actual symmetry of the CRDM nozzle layout is quarter rotational symmetry. The eighth of the head modeled results in one additional CRDM penetration in each quadrant, which conservatively removes more material (i.e., there is less metal available to carry the applied loadings) and has negligible effect on the applicability of the symmetry boundary condition due to the size of the penetration compared to the size of the head.

3.3 Modeling Simplifications

The following modeling simplifications are used in this calculation:

1. The geometry of the J-groove weld and butter is simplified to allow for a high quality mesh in this area and insertion of the crack tip elements needed to calculate stress intensity factors. Simplifications include the "kink" in the crack fronts rather than a smooth radius and neglecting the small fillet weld. These simplifications are typical of these types of analysis and do not impact the results.
2. For the limit load analysis (Section 6.5.1), the material removed to represent the J-groove weld, butter and crack growth has a simplified geometry to facilitate modeling. This simplification has no impact since acceptable area is removed.

4.0 DESIGN INPUTS

4.1 Geometry

The existing geometry of the RVCH and J-groove weld(s) for each unit are show in References [7], [8], [9], [10], [11], [12], [13], and [14]. The proposed repair configuration is provided in References [15] and [16]. Key dimensions are listed in Table 4-1.

Table 4-1: Key Dimensions

Description	Value	Reference/Comments
Head Inside Radius to Cladding	[ ]	[16]
Head Thickness	[ ]	[16]
Cladding Thickness	[ ]	[16]
Bore Diameter	[ ]	[16]
Horizontal Radius to Outermost Penetration	[ ]	[16]

4.2 Materials

4.2.1 Material Specifications

The material designations of each component are listed in Table 4-2.

Table 4-2: Component Materials

Component	Material	Reference/Comments
RVCH	[ ]	Reference [1]
Cladding	[ ]	Reference [6], Equip. Spec 676413
Existing J-Groove Weld/Buttering	[ ]	Reference [1]

4.2.2 Mechanical Material Properties

The material properties are taken from the original construction code, Reference [17]. The material properties for each component are provided in Table 4-3, Table 4-4, and Table 4-5. The [ ] properties are also used for the [ ] weld filler metals.

Table 4-3: RVCH Material Properties

[ ]					
Temperature (°F)	α (1/°F)	E (psi)	ν (-)	σ_y (ksi)	σ_u (ksi)
[ ]					
Reference [17] Location	Table I-5.0, Coeff. B	Table I-6.0	Typical	Table I-2.1	Table I-1.1

Table 4-4: J-Groove Weld, and Butter Material Properties

Temperature (°F)	α (1/°F)	E (psi)	v (-)	σ_y (ksi)	σ_u (ksi)
[					]
Reference [17] Location	Table I-5.0, Coeff. B	Table I-6.0	Typical	Table I-2.2	Table I-1.2

Table 4-5: Cladding Material Properties

Temperature (°F)	α (1/°F)	E (psi)	v (-)
[			]
Reference [17] Location	Table I-5.0, Coeff. B	Table I-6.0	Typical

4.2.3 Fracture Material Properties

Table 4-6 provides the reference temperature for nil-ductility (RT_{NDT}), and the sulfur content for the closure head center disc for each of the four units (Reference [18]). The analysis performed in this calculation uses the bounding values of all units, which is an RT_{NDT} of [ ]

Table 4-6: Fracture Material Properties

Plant	Unit	Heat No.	RT_{NDT} (°F)	Sulfur (wt %)
Byron	1	C3486-1	[ ]	[ ]
Byron	2	C4375-2	[ ]	[ ]
Braidwood	1	D1398-1	[ ]	[ ]
Braidwood	2	B9754-1	[ ]	[ ]

Reference [18] provides an estimate of the Charpy V-notch upper-shelf energy (USE) which is based on the average energy from CVN tests at RT_{NDT}+60°F. Review of the Charpy data provided in the CMTRs attached to Reference [18] indicates that this is a very conservative estimate of USE, as the percent shear fractures range from 50%-60% at this level. Per Reference [20], USE is defined by ASTM E185 (Reference [19]), which provides the following definition of the USE:

> *Charpy upper-shelf energy level*—the average energy value for all Charpy specimen tests (preferably three or more) whose test temperature is at or above the Charpy upper-shelf onset; specimens tested at temperatures greater than 83°C (150°F) above the Charpy upper-shelf onset shall not be included, unless no data are available between the onset temperature and onset +83°C (+150°F).
>
> *Charpy upper-shelf onset*—the test temperature above which the fracture appearance of all Charpy specimens tested is at or above 95% shear.

The CVN test data from the CMTRs is provided in Table 4-7. From Table 4-7, a lower bound USE of [ ] is selected based on the Braidwood 1 data at [ ] where the percent shear fracture is [ ] Note that the use of data at [ ] shear fracture is still conservative relative to the ASTM definition of 95% shear fracture.

Table 4-7: CVN Test Data

Plant	Temperature (°F)	Energy (ft-lbs)				Percent Shear Fracture		
		Test 1	Test 2	Test 3	Average	Test 1	Test 2	Test 3
Byron 1	212							
Byron 1	100							
Byron 1	70							
Byron 1	50							
Byron 1	40							
Byron 1	10							
Byron 1	-150							
Byron 2	212							
Byron 2	100							
Byron 2	80							
Byron 2	60							
Byron 2	20							
Byron 2	-50							
Byron 2	-100							
Braidwood 1	212							
Braidwood 1	***60***							
Braidwood 1	30							
Braidwood 1	0							
Braidwood 1	-30							
Braidwood 1	-60							
Braidwood 1	-100							
Braidwood 2	212							
Braidwood 2	70							
Braidwood 2	60							
Braidwood 2	0							
Braidwood 2	-10							
Braidwood 2	-20							
Braidwood 2	-60							

From Article A-4200 of Reference [2], the lower bound fracture toughness for crack arrest, K_{Ia}, is calculated as

$$K_{Ia} = 26.8 + 12.445\exp[0.0145(T - RT_{NDT})]$$

where T is the crack tip temperature, K_{Ia} is in units of ksi$\sqrt{in}$, and T and RT_{NDT} are in units of °F. In the present calculations, K_{Ia} is limited to a maximum value of 200 ksi$\sqrt{in}$ (upper-shelf fracture toughness). The crack arrest K_{Ia} upper shelf toughness of 200 ksi$\sqrt{in}$ is achieved at T-RT_{NDT} > 182 °F.

A higher measure of fracture toughness is provided by the K_{IC} fracture toughness for crack initiation, approximated in Article A-4200 of Section XI (Reference [2]) by

$$K_{Ic} = 33.2 + 20.734\exp[0.02(T - RT_{NDT})]$$

The crack initiation K_{IC} upper shelf toughness of 200 ksi$\sqrt{in}$ is achieved at T-RT_{NDT} > 105 °F.

The J-integral resistance (J-R) curve, needed for the EPFM method of analysis, is obtained from the following correlation for reactor pressure vessel plate with less than 0.018 weight percent sulfur (Reference [20], Section 3.3.1)

$$J_{mat} = MF\{C_1(\Delta a)^{C_2}\exp(C_3(\Delta a)^{C_4})\}$$

where MF is a margin factor, and Δa is the crack extension. C_i are constants which depend on the crack tip temperature and the Charpy V-notch upper-shelf energy as defined below

$$C_1 = \exp(-2.44 + 1.13\ln(CVN) - 0.00277T)$$

$$C_2 = 0.077 + 0.116\ln C_1$$

$$C_3 = -0.0812 - 0.0092\ln C_1$$

$$C_4 = -0.409$$

where CVN is the Charpy V-notch upper-shelf energy in ft-lbs, and T is the crack tip temperature in °F. In this analysis the margin factor, MF, is taken as 0.749 for all cases including faulted where it may be taken as one. The resulting material J-R curve is plotted for several temperatures in Figure 4-1.

Figure 4-1: J-R Curves as a Function of Temperature

The material tearing modulus is calculated using the following equation

$$T_{mat} = \left(\frac{E}{\sigma_f^2}\right)\frac{\partial J_{mat}}{\partial a}$$

where E is the Elastic Modulus, σ_f is the flow stress defined as $0.5(\sigma_y + \sigma_u)$, and the derivative of the J-R curve is

$$\frac{\partial J_{mat}}{\partial a} = MF\{C_1C_2(\Delta a)^{C_2-1} + C_1C_3C_4(\Delta a)^{C_2+C_4-1}\}\exp(C_3(\Delta a)^{C_4})$$

4.3 Transients

Fatigue crack growth will be calculated for the Normal and Upset transients listed in Table 4-8, based on Table 4-6 of the Section III analysis (Reference [22]). Per Reference [6] (TODI-BYR-15-008) the design cycles specified are applicable for a [ ] life.

Table 4-8: Transients

Transient	Abbreviation	Service Level	Cycles	Cycles/Year
		Normal		
		Normal		
		Normal		
		Normal		
		Normal		
		Upset		
		Upset		
		Upset		
		Upset		
		Upset		
		Upset		
		Upset		
		Upset		
		Upset		
		Test		
		Test		

* The [ ] transient is addressed in Appendix C.

Additionally, the Emergency and Faulted transient pressure temperature curves provided in Reference [6] (TODI BYR-15-009 & TODI BYR-15-012) were reviewed and the critical transients were selected for analysis based on the discussion below in Table 4-9. Emergency and Faulted transients have a small number of cycles (5 or less) and are therefore not considered for fatigue.

Table 4-9: Emergency and Faulted Transients

4.4 Finite Element Model

The finite element model utilized is a three-dimensional half symmetry model. The model is meshed using ANSYS element types SOLID186 and SOLID187. The crack tip elements are SOLID186 elements collapsed into wedges with the appropriate mid-side nodes moved to the quarter points to simulate the singularity at the crack tip. A base geometry and mesh are generated in the input file "base_model.inp", and the explicit crack models are then created by replacing the appropriate brick elements with crack tip elements using the files "gen_crack_models.inp" and "CrackFanMesh2.mac".

4.4.1 Boundary Conditions

The displacements are constrained normal to the face of the symmetry plane and the additional model cutting planes. The displacements of the nodes on the crack face are not constrained.

4.4.2 Applied Stresses

Applied stresses are due to residual stresses and operating stresses. Residual stresses are obtained from the 3-D weld residual stress calculation documented in Reference [21]. Stresses are mapped to the crack face from the residual stress model to the crack finite element model through arrays of nodal locations and hoop stresses documented in Appendix B of Reference [21]. Figure 4-2 shows an example of the weld residual stresses mapped onto downhill crack face 1 side by side with contour plot of the stress from Reference [21]. Operating stresses are taken from the corresponding ASME Section III calculation (Reference [22]) and mapped to the crack face using the same methodology as the residual stresses. The operating pressure is also applied to the crack face to account for the additional loading.

The files used for stress results from References [21] and [22] are listed in Table 4-10.

Table 4-10: Stress Result Files

Load	Stress File
[ ]	

Figure 4-2: Weld Residual Stress Mapped to Downhill Crack Front 1

5.0 COMPUTER FILES

5.1 Software

ANSYS Version 14.5.7 (Reference [23]) was used in this analysis. Error notices were reviewed and none are applicable to the features utilized in this analysis, therefore, the use of this version is acceptable. All modeling and analyses were performed on the following computer:

- DELL Precision M6600, Intel(R) Core(TM) i7-2640M CPU @ 2.80GHz, 8GB of RAM
- Operating System: Windows 7, Service Pack 1, 64 Bit
- Name of person running tests: Tom Riordan
- Date of Tests Before Runs: February 23, 2015
- Date of Tests After Runs: May 1, 2015
- Date of Test for Rev 002 Runs: August 24, 2016 (verification test performed at same time as runs).

The test problem vm143 was run before and after the analysis and the results were found to be acceptable as documented in output files "vm143.out" and "vm143.vrt" (see Table 5-1). The test problem vm143 was also run for revision 002 and is documented in output files "vm143.out" and "vm143.vrt" (see Table 5-2).

5.2 Computer Files

The computer files for runs performed in revision 000 are listed in Table 5-1. The files for revision 002 are listed in Table 5-2. Files are stored in ColdStor at the following paths:

\cold\General-Access\32\32-9000000\32-9236713-000\official (Table 5-1)

\cold\General-Access\32\32-9000000\32-9236713-002\official (Table 5-2)

Table 5-1: Computer Files

CRC Checksum	File Size (bytes)	Modified Date	Time	File Name
./KI:				
21263	1578	Mar 9 2015	20:49:48	Design_dh1.KI
60449	1578	Mar 9 2015	22:18:41	Design_dh2.KI
43257	1578	Mar 9 2015	17:40:33	Design_uh1.KI
07900	1578	Mar 9 2015	19:10:35	Design_uh2.KI
21104	3300	Feb 10 2015	12:36:22	Get_SIF.mac
03319	3386	Feb 23 2015	19:08:04	SIF_Driver.mac
14846	326	Feb 23 2015	10:06:44	SIF_calc.inp
03910	82149439	Mar 10 2015	0:04:51	SIF_calc.out
43416	6838	Mar 9 2015	20:52:58	Tr_CD_st_dh1.KI
31139	6838	Mar 9 2015	22:22:30	Tr_CD_st_dh2.KI
24024	6838	Mar 9 2015	17:43:46	Tr_CD_st_uh1.KI
33054	6838	Mar 9 2015	19:14:07	Tr_CD_st_uh2.KI

CRC Checksum	File Size (bytes)	Modified Date	Time	File Name
26871	9994	Mar 9 2015	20:57:50	Tr_CRD_st_dh1.KI
49184	9994	Mar 9 2015	22:28:22	Tr_CRD_st_dh2.KI
23505	9994	Mar 9 2015	17:48:41	Tr_CRD_st_uh1.KI
60584	9994	Mar 9 2015	19:19:32	Tr_CRD_st_uh2.KI
18031	8416	Mar 9 2015	21:01:51	Tr_CREJ_st_dh1.KI
08844	8416	Mar 9 2015	22:33:12	Tr_CREJ_st_dh2.KI
52638	8416	Mar 9 2015	17:52:46	Tr_CREJ_st_uh1.KI
40552	8416	Mar 9 2015	19:24:00	Tr_CREJ_st_uh2.KI
01489	7890	Mar 9 2015	21:05:35	Tr_FWC_st_dh1.KI
05454	7890	Mar 9 2015	22:37:41	Tr_FWC_st_dh2.KI
59732	7890	Mar 9 2015	17:56:33	Tr_FWC_st_uh1.KI
41752	7890	Mar 9 2015	19:28:39	Tr_FWC_st_uh2.KI
39983	5786	Mar 9 2015	21:08:10	Tr_HU_st_dh1.KI
44194	5786	Mar 9 2015	22:40:46	Tr_HU_st_dh2.KI
00116	5786	Mar 9 2015	17:59:10	Tr_HU_st_uh1.KI
24397	5786	Mar 9 2015	19:31:30	Tr_HU_st_uh2.KI
22332	1578	Mar 9 2015	21:08:28	Tr_HYDR_st_dh1.KI
58287	1578	Mar 9 2015	22:41:07	Tr_HYDR_st_dh2.KI
33547	1578	Mar 9 2015	17:59:28	Tr_HYDR_st_uh1.KI
34672	1578	Mar 9 2015	19:31:50	Tr_HYDR_st_uh2.KI
16128	7890	Mar 9 2015	21:12:12	Tr_IDPR_st_dh1.KI
58366	7890	Mar 9 2015	22:45:34	Tr_IDPR_st_dh2.KI
37100	7890	Mar 9 2015	18:03:14	Tr_IDPR_st_uh1.KI
05728	7890	Mar 9 2015	19:35:58	Tr_IDPR_st_uh2.KI
12377	14202	Mar 9 2015	21:19:22	Tr_ISI_st_dh1.KI
60741	14202	Mar 9 2015	22:54:12	Tr_ISI_st_dh2.KI
50307	14202	Mar 9 2015	18:10:30	Tr_ISI_st_uh1.KI
45145	14202	Mar 9 2015	19:43:57	Tr_ISI_st_uh2.KI
16826	7890	Mar 9 2015	21:23:06	Tr_IST_st_dh1.KI
20455	7890	Mar 9 2015	22:58:40	Tr_IST_st_dh2.KI
47038	7890	Mar 9 2015	18:14:18	Tr_IST_st_uh1.KI
04858	7890	Mar 9 2015	19:48:05	Tr_IST_st_uh2.KI
53576	2630	Mar 9 2015	21:23:58	Tr_LEAK_st_dh1.KI
63228	2630	Mar 9 2015	22:59:43	Tr_LEAK_st_dh2.KI
18199	2630	Mar 9 2015	18:15:10	Tr_LEAK_st_uh1.KI
13851	2630	Mar 9 2015	19:49:03	Tr_LEAK_st_uh2.KI
50913	13150	Mar 9 2015	21:30:34	Tr_LOF_st_dh1.KI
01496	13150	Mar 9 2015	23:07:38	Tr_LOF_st_dh2.KI
11614	13150	Mar 9 2015	18:21:52	Tr_LOF_st_uh1.KI
48527	13150	Mar 9 2015	19:56:23	Tr_LOF_st_uh2.KI
35510	8942	Mar 9 2015	21:34:53	Tr_LOP_st_dh1.KI
15662	8942	Mar 9 2015	23:12:49	Tr_LOP_st_dh2.KI

CRC Checksum	File Size (bytes)	Modified Date			Time	File Name
13722	8942	Mar	9	2015	18:26:14	Tr_LOP_st_uh1.KI
56332	8942	Mar	9	2015	20:01:10	Tr_LOP_st_uh2.KI
54380	9994	Mar	9	2015	21:39:45	Tr_LSB_st_dh1.KI
37299	9994	Mar	9	2015	23:18:39	Tr_LSB_st_dh2.KI
22926	9994	Mar	9	2015	18:31:11	Tr_LSB_st_uh1.KI
07182	9994	Mar	9	2015	20:06:37	Tr_LSB_st_uh2.KI
31946	10520	Mar	9	2015	21:44:56	Tr_LSLD_st_dh1.KI
37662	10520	Mar	9	2015	23:24:52	Tr_LSLD_st_dh2.KI
28612	10520	Mar	9	2015	18:36:27	Tr_LSLD_st_uh1.KI
53332	10520	Mar	9	2015	20:12:24	Tr_LSLD_st_uh2.KI
46341	9468	Mar	9	2015	21:49:30	Tr_PL_st_dh1.KI
16512	9468	Mar	9	2015	23:30:22	Tr_PL_st_dh2.KI
43281	9468	Mar	9	2015	18:41:07	Tr_PL_st_uh1.KI
26618	9468	Mar	9	2015	20:17:29	Tr_PL_st_uh2.KI
41536	9994	Mar	9	2015	21:54:23	Tr_PU_st_dh1.KI
30086	9994	Mar	9	2015	23:36:14	Tr_PU_st_dh2.KI
25843	9994	Mar	9	2015	18:46:03	Tr_PU_st_uh1.KI
30445	9994	Mar	9	2015	20:22:56	Tr_PU_st_uh2.KI
57260	7364	Mar	9	2015	21:57:49	Tr_RCPB_st_dh1.KI
45070	7364	Mar	9	2015	23:40:20	Tr_RCPB_st_dh2.KI
15759	7364	Mar	9	2015	18:49:33	Tr_RCPB_st_uh1.KI
19950	7364	Mar	9	2015	20:26:46	Tr_RCPB_st_uh2.KI
39199	10520	Mar	9	2015	22:03:00	Tr_RT_st_dh1.KI
02804	10520	Mar	9	2015	23:46:34	Tr_RT_st_dh2.KI
42095	10520	Mar	9	2015	18:54:48	Tr_RT_st_uh1.KI
17981	10520	Mar	9	2015	20:32:30	Tr_RT_st_uh2.KI
00064	8416	Mar	9	2015	22:07:02	Tr_SLD_st_dh1.KI
31844	8416	Mar	9	2015	23:51:23	Tr_SLD_st_dh2.KI
42805	8416	Mar	9	2015	18:58:53	Tr_SLD_st_uh1.KI
26036	8416	Mar	9	2015	20:36:59	Tr_SLD_st_uh2.KI
05984	8942	Mar	9	2015	22:11:21	Tr_SLI_st_dh1.KI
11211	8942	Mar	9	2015	23:56:34	Tr_SLI_st_dh2.KI
36053	8942	Mar	9	2015	19:03:15	Tr_SLI_st_uh1.KI
15136	8942	Mar	9	2015	20:41:48	Tr_SLI_st_uh2.KI
29896	7890	Mar	9	2015	22:15:09	Tr_SSB_st_dh1.KI
43498	7890	Mar	10	2015	0:01:02	Tr_SSB_st_dh2.KI
11972	7890	Mar	9	2015	19:07:02	Tr_SSB_st_uh1.KI
13532	7890	Mar	9	2015	20:45:59	Tr_SSB_st_uh2.KI
32334	6838	Mar	9	2015	22:18:19	Tr_TRT_st_dh1.KI
64867	6838	Mar	10	2015	0:04:50	Tr_TRT_st_dh2.KI
16300	6838	Mar	9	2015	19:10:15	Tr_TRT_st_uh1.KI
01608	6838	Mar	9	2015	20:49:30	Tr_TRT_st_uh2.KI

CRC Checksum	File Size (bytes)	Modified Date			Time	File Name
12170	845	Feb	10	2015	12:36:04	calc_k.mac
./KI_WRS:						
21104	3300	Feb	10	2015	12:36:22	Get_SIF.mac
53662	2385	Mar	26	2015	17:38:40	SIF_Driver_WRS.mac
58341	342	Mar	26	2015	17:36:31	SIF_calc.inp
40929	342533	Mar	26	2015	17:40:17	SIF_calc.out
21270	864600	Mar	26	2015	16:42:36	WRS_JG.out
14702	1578	Mar	26	2015	17:39:55	WRS_dh1.KI
19074	1578	Mar	26	2015	17:40:16	WRS_dh2.KI
45110	1578	Mar	26	2015	17:39:17	WRS_uh1.KI
02636	1578	Mar	26	2015	17:39:37	WRS_uh2.KI
12170	845	Feb	10	2015	12:36:04	calc_k.mac
./Limit_Load:						
43418	14478341	May	1	2015	7:52:06	BB_Head_Eighth_Symm_geom.inp
08136	2497	May	1	2015	7:53:31	BB_Head_LL.inp
14343	388270	May	1	2015	8:28:27	BB_Head_LL.out
24444	1183	May	1	2015	9:03:30	Sphere_LL.inp
34694	111381	May	1	2015	9:22:43	Sphere_LL.out
59712	12824244	May	1	2015	8:54:56	Sphere_geom.inp
52686	10355	Apr	9	2015	16:38:20	materials_LL.inp
./Model:						
46075	9664611	Feb	9	2015	11:22:02	Base_Model.inp
08317	6653	Dec	16	2013	9:41:18	CrackFanMesh2.mac
50705	8654	Feb	10	2015	12:03:02	gen_crack_models.inp
55233	669743	Feb	23	2015	16:03:11	gen_crack_models.out
31314	9917	Dec	11	2013	17:45:05	materials.inp
./Spreadsheets:						
21706	144488	May	1	2015	10:02:13	BB_Weld_Removed_Area.xlsx
30682	558077	Apr	8	2015	11:39:32	EPFM-RG1161_dh.xlsm
38937	557641	Apr	8	2015	11:22:11	EPFM-RG1161_uh.xlsm
32149	397032	Apr	8	2015	11:40:41	LEFM_FCG_dh.xlsm
04536	376452	Apr	8	2015	11:22:16	LEFM_FCG_uh.xlsm
./Verification/Post:						
34097	14718	Mar	16	2013	18:00:53	vm143.dat
48177	100295	May	1	2015	10:17:48	vm143.out
39033	766	May	1	2015	10:17:48	vm143.vrt

CRC Checksum	File Size (bytes)	Modified Date			Time	File Name
./Verification/Pre:						
34097	14718	Mar	16	2013	18:00:53	vm143.dat
41169	100534	Feb	23	2015	9:23:05	vm143.out
39033	766	Feb	23	2015	9:23:05	vm143.vrt

Table 5-2: Computer Files for Rev 002

CRC Checksum	File Size (bytes)	Modified Date			Time	File Name
./KI:						
21104	3300	Feb	10	2015	12:36:22	Get_SIF.mac
39664	3414	Aug	24	2016	15:09:47	SIF_Driver.mac
14846	326	Feb	23	2015	10:06:44	SIF_calc.inp
48138	5868595	Aug	24	2016	15:48:25	SIF_calc.out
33487	12624	Aug	24	2016	15:40:48	Tr_EFT_st_dh1.KI
62660	12624	Aug	24	2016	15:48:24	Tr_EFT_st_dh2.KI
13457	12624	Aug	24	2016	15:27:33	Tr_EFT_st_uh1.KI
42858	12624	Aug	24	2016	15:34:29	Tr_EFT_st_uh2.KI
12170	845	Feb	10	2015	12:36:04	calc_k.mac
./Spreadsheets:						
37043	580898	Sep	15	2016	16:12:23	EPFM-RG1161_dh_EFT.xlsm
58915	580927	Sep	9	2016	11:29:58	EPFM-RG1161_uh_EFT.xlsm
40908	402698	Sep	15	2016	16:12:29	LEFM_FCG_dh_EFT.xlsm
18412	379945	Sep	9	2016	11:29:45	LEFM_FCG_uh_EFT.xlsm
./Verification:						
34097	14718	Mar	16	2013	18:00:53	vm143.dat
09679	100295	Aug	24	2016	15:14:41	vm143.out
39033	766	Aug	24	2016	15:14:41	vm143.vrt

6.0 CALCULATIONS

6.1 Stress Intensity Factors

SIFs are calculated for each postulated crack front using the WRS and Section III stress results from the files listed in Table 4-10. The calculations are run by the ANSYS input file "SIF_calc.inp". The ANSYS macros "SIF_Driver.mac" and "SIF_Driver_WRS.mac" set the crack face boundary conditions, read in data from the stress models (WRS or Section III), and set up data arrays. The file "Get_SIF.mac" is used to perform stress mapping, solve the model with mapped stresses and then calculate the SIFs (using "calc_k.mac"). The SIF calculation results are written to the "*.KI" output files (see Table 5-1), which contain the SIFs for each step of a transient as well as a summary of the minimum and maximum SIF for the transient.

Upon reviewing the results of the uphill stress intensity factor calculations for the Design Condition it was seen that at positions near the bore (e.g., 16 and 17) the stress intensity factor is lower at crack front 2 than crack front 1; this is a result of the fact that stress results from the Section III model include additional constraint from the IDTB weld which is near the uphill crack front 2. In cases where the hillside angle is less steep the IDTB weld may not be as near to the J-groove weld. Therefore, it was decided that for conservatism the uphill crack front 2 results would not be used in calculations; instead, the stress intensity factors at flaw sizes larger than uphill crack front 1 will be conservatively extrapolated using the scaling rule described in Section 2.1.

The simplified geometry of the postulated flaw shapes discussed in simplification 1 of Section 3.3 results in low SIFs at some locations along the crack front (see tabulated values in Appendix A and Appendix B) such as at the "kink" at position 9 on the uphill side (Figure 2-2), and near the head ID surface at position 1 on the downhill side (Figure 2-3). The low values in these areas result because crack tip opening at these locations is restrained by other portions of the crack front due to the postulated flaw geometry. This has no impact on the results since these are not the controlling locations.

The boundary conditions utilized (Section 4.4.1) release the nodes on the crack face; in cases where there is compressive stress the crack face may close (i.e., move across the symmetry plane) producing positive SIFs where there should not be. For example, on uphill crack face 1, closure occurs only in one of the steps of the [ ] transient. This closure results in small positive values ([ ] at position 17) that are near the minimum. The positive value predicted during closure would have a minor impact on the fatigue crack growth due to larger delta K, but with a beneficial effect of smaller R ratio. Very localized closure also occurs near the surface in transients such as a [ ] transient where there is a rapid increase in the temperature causing a compressive skin stress; in this case, the majority of the crack face remains open, and therefore would only be minimally affected. The overall effect on the analysis due to the small amount of crack face closure observed is minimal.

6.2 Fatigue Crack Growth

Utilizing the SIF solutions described in Section 6.1, fatigue crack growth is calculated. The fatigue crack growth rule in Section 2.2 is integrated numerically using,

$$\frac{da}{dN} \approx \frac{\Delta a}{\Delta N} \approx C_0(\Delta K_I)^n, \quad or \quad \Delta a \approx \Delta N C_0(\Delta K_I)^n$$

The impact of the cycle increment (ΔN) was investigated, and it was found that utilizing the number of cycles per year was a sufficiently small increment to accurately integrate the crack growth. Therefore, crack growth presented in this report has been calculated on a per year basis.

Based on review of the results, the stress intensity factors at position 17 at the nozzle bore on both the uphill and downhill side are typically largest. Exceptions to this occur in transients with rapid temperature drops which create high thermal stresses near the ID of the RVCH. The subsequent EPFM analyses will apply lower safety factors to these secondary stresses. Therefore, the nozzle bore locations are considered bounding and chosen for detailed evaluation. Fatigue crack growth calculations for position 17 on the uphill side and position 17 on the downhill side are performed in the spreadsheets "LEFM_FCG_uh.xlsm" and "LEFM_FCG_dh.xlsm" (see Table 5-1), and the detailed results are shown in Appendix A and Appendix B, respectively.

6.3 LEFM Evaluation

LEFM evaluations are performed for the final flaw size from the fatigue crack growth evaluation. The applied SIF is evaluated accounting for the plastic zone correction described in Section 2.1.1, and its acceptability is evaluated based on the rules outlined in Section 2.3. The results for uphill position 17 and downhill position 17 are shown in Table 6-1 and Table 6-2, respectively.

Table 6-1: Uphill Position 17 LEFM Results

RT_{NDT}	[ ]	°F
T_C	[ ]	°F
Upper Shelf Toughness	200	ksiVin
Initial Flaw Size, a_i	[ ]	in
Final Flaw Size, a_f	[ ]	in
Crack Growth, Δa	[ ]	in

Loading	[
Service Level	
Temperature (°F)	
Pressure (psi)	
Sy (ksi)	
K_{Ic} (ksiVin)	
K_{Ia} (ksiVin)	
K(a) (ksiVin)	
a_e (in)	
$K(a_e)$ (in)	
Margin = $K_{Ic}/K(a_e)$	
Margin = $K_{Ia}/K(a_e)$	
Required Margin	
Acceptable By LEFM?	
Meets T_C Criterion for EPFM?	]

Table 6-2: Downhill Position 17 LEFM Results

RT_{NDT}	[ ]	°F
T_C	[ ]	°F
Upper Shelf Toughness	200	ksiVin
Initial Flaw Size, a_i	[ ]	in
Final Flaw Size, a_f	[ ]	in
Crack Growth, Δa	[ ]	in

Loading	[
Service Level	
Temperature (°F)	
Pressure (psi)	
Sy (ksi)	
K_{Ic} (ksiVin)	
K_{Ia} (ksiVin)	
K(a) (ksiVin)	
a_e (in)	
K(a_e) (in)	
Margin = K_{Ic}/K(a_e)	
Margin = K_{Ia}/K(a_e)	
Required Margin	
Acceptable By LEFM?	
Meets T_C Criterion for EPFM?	]

Review of the results of Table 6-1 and Table 6-2 indicates that with few exceptions the LEFM acceptance criteria are not met; however, in all cases shown except the Hydrostatic test and the [ ] the temperature exceeds [ ] and may therefore be analyzed based on EPFM. The cases of the Hydrostatic test and the RCPB are addressed below.

For the Hydrostatic test case the LEFM results are not acceptable and the temperature considered of [ ] does not meet the criteria to be analyzed by EPFM. Since the Hydrostatic test is a controlled event and the test temperature is chosen, a temperature of [ ] will be considered and EPFM analysis will be performed. The Hydrostatic test case will be considered acceptable subject to meeting the EPFM requirements provided that Hydrostatic tests are performed with metal temperature of [ ] of greater.

The [ ] results listed in Table 6-1 and Table 6-2 also do not meet the LEFM criteria or the T_c criteria to be analyzed by EPFM; however, Table 6-1 and Table 6-2 have conservatively used the fluid temperature used in the Section III analysis and not the metal temperatures. For the uphill side the maximum stress intensity factor occurs at step 11, which from Table 6-4 of Reference [22] is a time of [ ] (note the downhill side maximum is earlier in the transient). From the detailed output in "Tr_RT_st.out" of Reference [22] at this time point the ID surface temperature is [ ] and the OD temperature is [ ] Linearly interpolating between the ID and OD, the temperature will with reach T_c at a depth of approximately [ ] On both the uphill and downhill side crack tip 17 is deeper than [ ] and the metal temperature will exceed T_c. Therefore the EPFM evaluations will be performed considering a metal temperature equal to T_c.

6.4 EPFM Evaluations

As noted in the previous section, the largest applied K is at the final flaw size; therefore, the EPFM evaluations will be performed for the final flaw size in accordance with the methodology described in Section 2.4 using the spreadsheets "EPFM-RG1161_uh.xlsm" and "EPFM-RG1161_dh.xlsm" (see Table 5-1). As discussed in the previous section all cases may be evaluated using EPFM. Table 6-3 and Table 6-4 provide the results of the EPFM evaluations. Note that when the higher safety factors provided in Section 3.1 of Code Case N-749 (Reference [3]) are used for the applied J-Integral criterion the stability check is not required; however, it is included here for completeness. As shown in Table 6-3 and Table 6-4, all cases meet the EPFM acceptance criteria. In all cases except for the [ ] transient on the downhill side the higher safety factors of Section 3.1 of Reference [3] are used; the safety factors of Section 3.2 of Reference [3] are used for the [ ] transient on the downhill side. Details of the calculations for the limiting [ ] transient are provided in Appendix A and Appendix B, for the uphill and downhill side, respectively.

In the EPFM evaluations, the K due to pressure (K_{IP}) is calculated based on the Design Condition results (Table A-2 and Table B-2). The Design Condition K is interpolated or extrapolated for the desired flaw size (see Section 2.1) and multiplied by the ratio of the transient pressure to the Design Pressure.

Table 6-3: Uphill Position 17 EPFM Results

	Loading
	Service Level
	Temperature (°F)
	Pressure (psi)
Applied J-Integral Check	Primary Safety Factor
	Secondary Safety Factor
	J_{app} (kips/in)
	$J_{0.1}$ (kips/in)
	Margin = $J_{0.1}/J_{app}$
	Required Margins
	Applied J-Integral Check Acceptable?
	Stability Check Required?
Stability Check	Primary Safety Factor
	Secondary Safety Factor
	T_{app}
	$T_{instability}$
	Margin = $T_{instability}/T_{app}$
	Required Margins
	Stability Check Acceptable?

Table 6-4: Downhill Position 17 EPFM Results

	Loading
	Service Level
	Temperature (°F)
	Pressure (psi)
Applied J-Integral Check	Primary Safety Factor
	Secondary Safety Factor
	J_{app} (kips/in)
	$J_{0.1}$ (kips/in)
	Margin = $J_{0.1}/J_{app}$
	Required Margins
	Applied J-Integral Check Acceptable?
	Stability Check Required?
Stability Check	Primary Safety Factor
	Secondary Safety Factor
	T_{app}
	$T_{instability}$
	Margin = $T_{instability}/T_{app}$
	Required Margins
	Stability Check Acceptable?

6.5 Primary Stress Evaluation

6.5.1 Limit Load Finite Element Model

The acceptance criterion of items 3.1(c) and 3.2(a)(3) of Reference [3] require that the primary stress limits of NB-3000 (Reference [24]) are met assuming a local area reduction of the pressure retaining membrane that is equal to the area of the flaw. As described in Section 2.5, the primary stress limits for design conditions (NB-3221.1, NB-3221.2, and NB-3221.3) need not be satisfied if it can be shown by performing a limit analysis (NB-3228.1) that the applied loadings do not exceed two-thirds of the lower bound collapse load. This condition is equivalent showing that the structure does not collapse at a pressure equal to 150% of the Design Pressure (1.5× [ ]). In terms of finite element results plastic collapse of the structure is equivalent to numerical instability.

The boundaries of the one nozzle model utilized for stress intensity factor calculations extend beyond half the distance between adjacent penetrations in some cases. As a result, the model cannot be used directly since it would potentially be taking credit for material that is needed to reinforce other penetrations; therefore, a new model has been developed considering a 45° sector of the head with all penetrations modeled. Since this is an approximation of the symmetry of the head an additional penetration is included to conservatively insure that the modeled configuration bounds all sectors. The model penetration layout is shown with the drawing in Figure 6-1. Each CRDM penetration is modeled with a diameter of [ ] (Reference [15]) and the vent line penetration is modeled with a diameter of [ ] corresponding to the OD of the [ ] (Reference [25]).

In order to represent the material removed by the postulated J-groove flaws and the crack growth the following method is used:

- A cut through the head is made at a depth of [ ] (center penetration max J-groove depth from base metal [12]) + [ ] (rounded up crack growth) = [ ] from the ID surface. This defines the depth of the metal removed.
- A cylindrical cut is made at each CRDM penetration to slice the material up to the [ ] depth. This volume of material is removed to represent the area of the flawed J-groove welds. A diameter of [ ] was selected for this cut. The cross-sectional area of these slices will be compared against the areas of the postulated flaws and projected crack growth later in this calculation to verify that this removes sufficient area.

The resulting model geometry with material removed is shown in Figure 6-2.

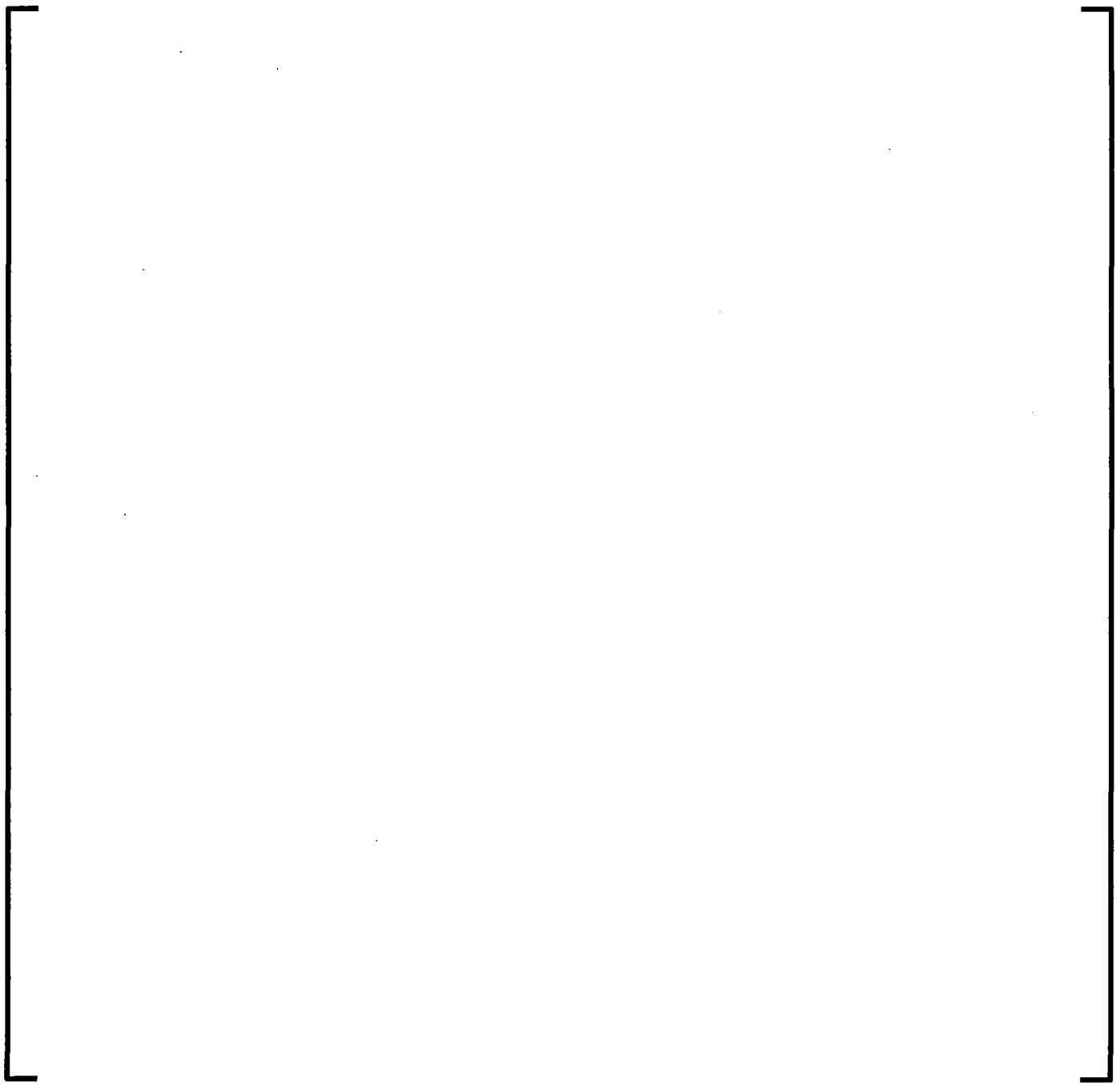

Figure 6-1: Limit Load Model Penetration Layout

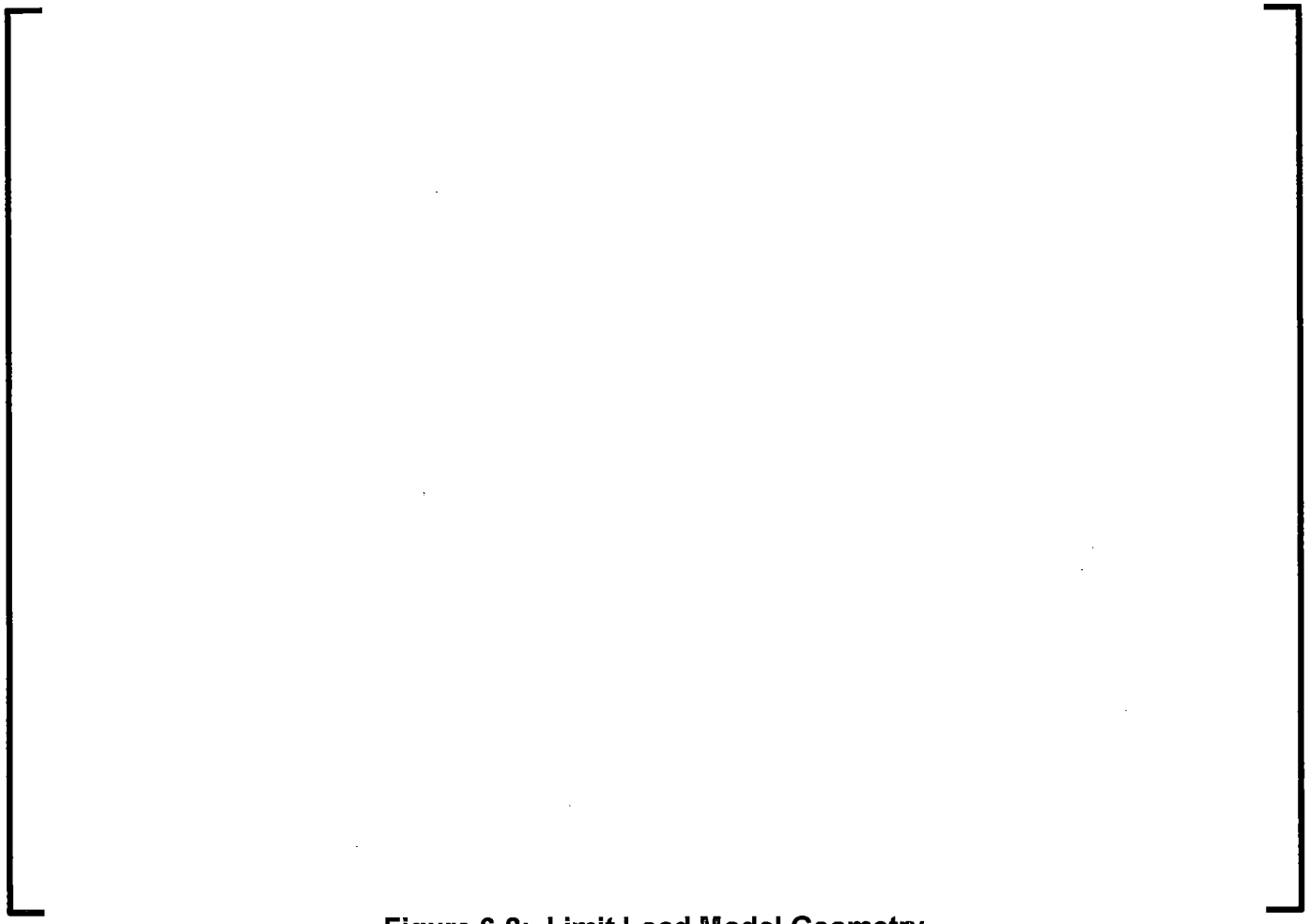

Figure 6-2: Limit Load Model Geometry

The overall model geometry and mesh are defined in the input file "BB_Head_Eighth_Symm_geom.inp" (see Table 5-1). The model is meshed with SOLID185 elements with [

] The finite element mesh utilized is shown in Figure 6-3.

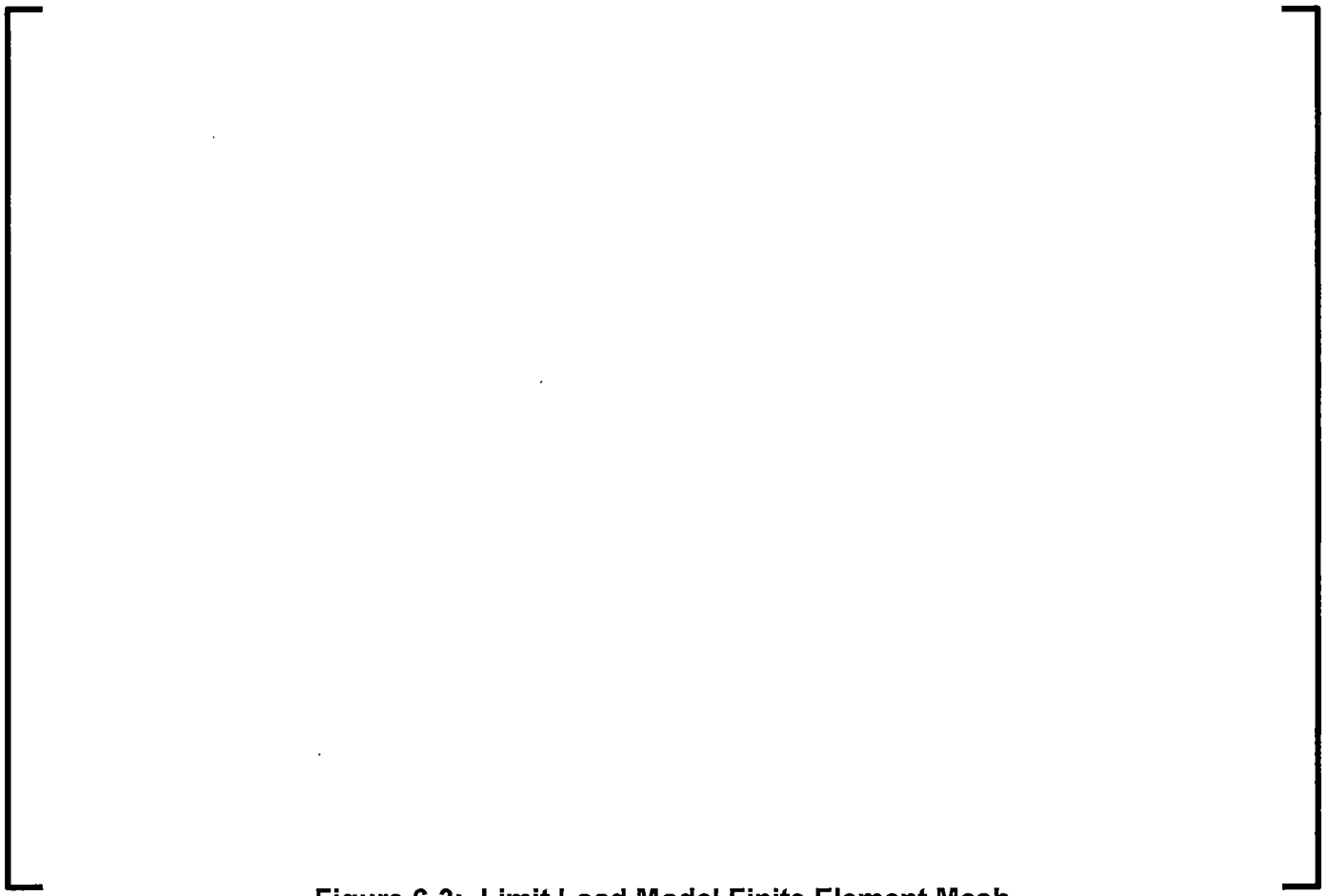

Figure 6-3: Limit Load Model Finite Element Mesh

The material properties for the analysis are defined in the file "materials_LL.inp". Note that the cladding and weld metal are excluded from the model since structural credit cannot be taken for the cladding and the weld metal is postulated to be flawed. The properties are identical to those used in the explicit crack models with the exception that the material has been changed to be elastic-perfectly plastic. The value of yield strength used is based on S_m (Reference [17]) the Design Temperature of [ ] and is given below.

RVCH (SA-533 Grade B Class 1) $S_y = 1.5S_m = 1.5(26.7 \text{ ksi}) = 40.05 \text{ ksi}$

Pressure is applied to the ID surface of the head and to the nozzle bores, incrementally increasing in each load step. Displacements normal to the three cut faces in the model are constrained. Additionally, end cap closure loads are accounted for by distributing the total load for each nozzle over the nozzle bore. The end cap loads are calculated using the following equation

[ ]

where P is the current applied pressure and d_{bore} is the bore diameter. When a nozzle falls on a cutting plane an appropriate fraction of the total load is utilized (i.e., half on the symmetry planes and one eighth for the center penetration).

The analysis is run using the input file "BB_Head_LL.inp" with results output to "BB_Head_LL.out". The output file shows the final converged load step at a pressure of [ ] which is equal to [ ] times the Design Pressure, which exceeds the requirement of 150% of the Design Pressure. The equivalent stress at the last converged load step is shown in Figure 6-4.

Figure 6-4: Equivalent Stresses at the Limit Pressure

6.5.1.1 Limit Load Methodology Verification

In order to verify that the modeling methodology utilized can accurately predict limit loads, a simplified test case of a spherical shell was run, and will be compared with the theoretical solution. The same model geometry was taken prior to cutting holes for penetrations and meshed with SOLID185 elements using similar mesh density and the same key options as the run described in 6.5.1. The model geometry and mesh are defined in the input file "Sphere_geom.inp". The finite element mesh for the test model is shown in Figure 6-5. The analysis is run by the input file "Sphere_LL.inp" (see Table 5-1).

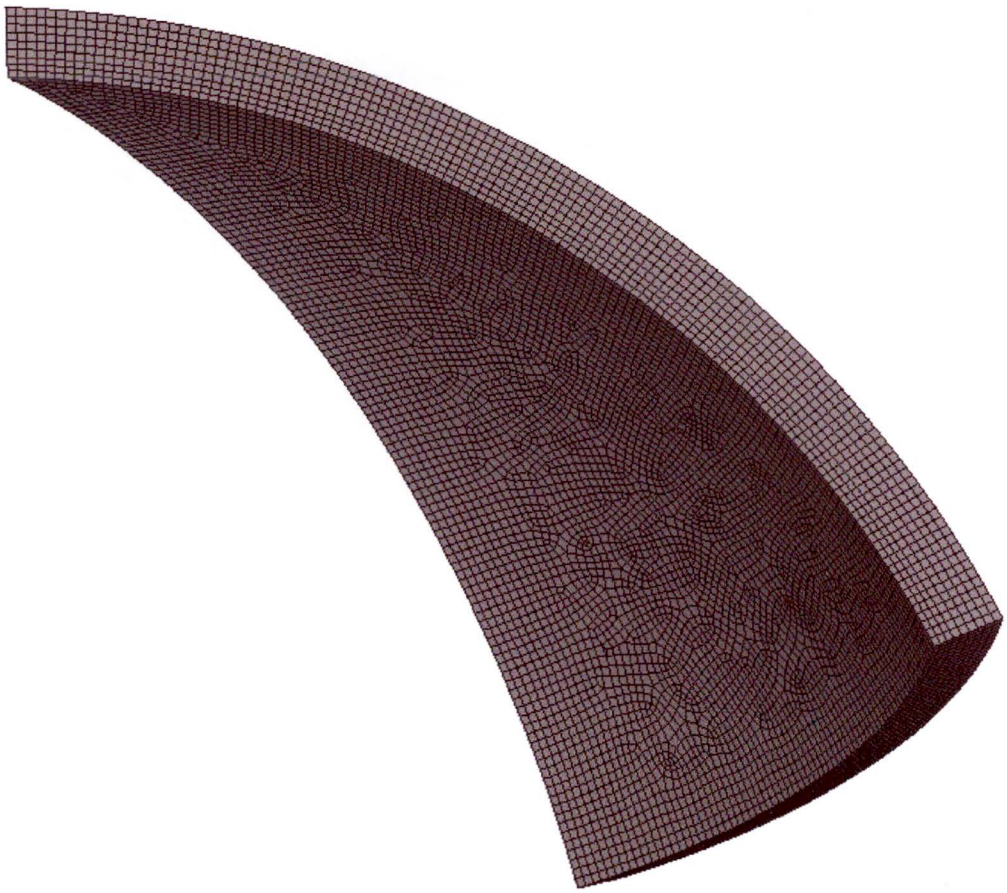

Figure 6-5: Finite Element Mesh for Limit Load Test Case

From the output file "Sphere_LL.out" the final converged solution is at a pressure of [ ] The equivalent stress at the limit pressure is shown in Figure 6-6.

The theoretical limit pressure for an elastic-perfectly plastic sphere loaded by internal pressure is given by (see e.g., Reference [26])

$$P_L = 2\sigma_y \ln\left(\frac{R_o}{R_i}\right)$$

where P_L is the limit pressure, σ_y is the yield strength, R_o is the outer radius, and R_i is the inner radius. For the test problem using the shell geometry described in Section 4.1this results in

[ ]

The finite element model predicted limit load of [ ] psig is equal to 99.5% of the theoretical solution above, which shows that the methodology utilized can accurately predict limit loads.

[ ]

Figure 6-6: Limit Load Test Case Equivalent Stress at Limit Pressure

6.5.2 Calculation of Flaw Area Removed

The cross-sectional areas of the material removed to represent the postulated J-groove flaws plus crack growth (see Figure 2-2 and Figure 2-3) on the uphill side and downhill side are calculated using the following equation (see for Figure 6-7 diagram)

[ ]

where x is the horizontal distance from the vessel centerline, R_1 is the inside radius of the vessel, and R_2 is the radius to the depth of the metal removed. In Figure 6-7, the area removed to represent the uphill flaw is indicated by area A2 and the downhill flaw by area A3. The integral is evaluated using the following solution from a table of integrals (e.g., Reference [27])

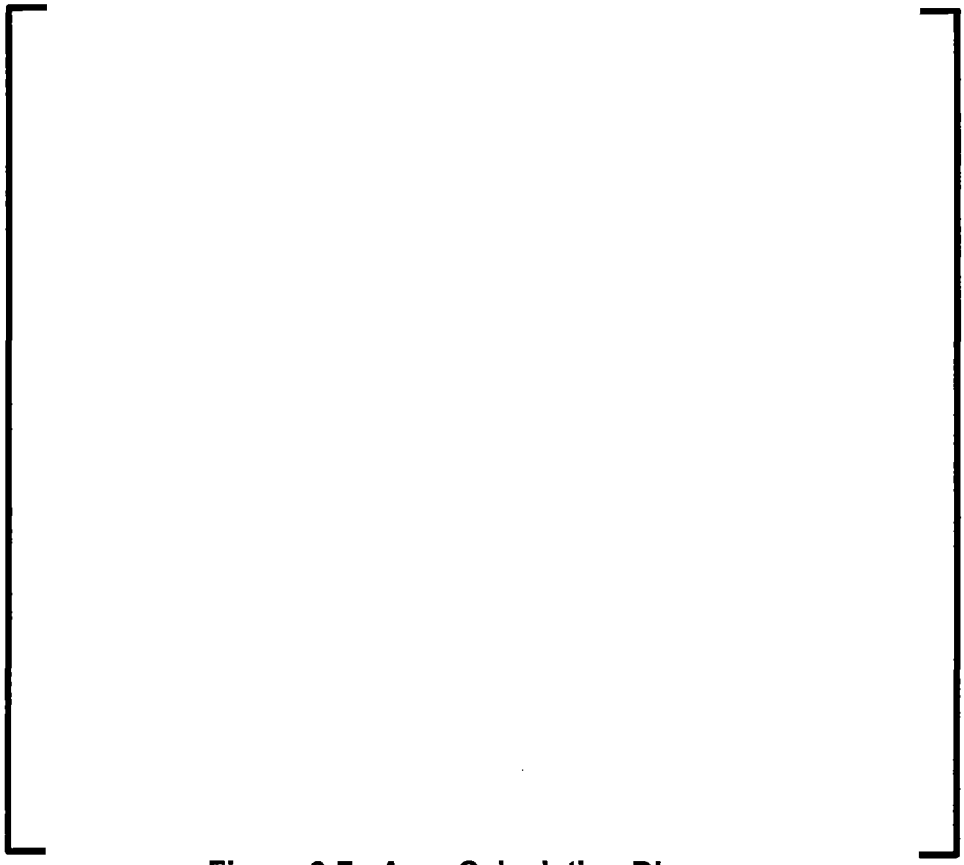

Figure 6-7: Area Calculation Diagram

The area removed from the ANSYS model is calculated in the spreadsheet "BB_Weld_Removed_Area.xlsx" (see Table 5-1) for the center penetration (1) and the outermost penetrations (74-78) since these will bound the minimum (center) and maximum (outermost) areas. The resulting areas removed from the ANSYS model are shown in Table 6-5.

Table 6-5: Model Areas Removed by the Cutouts to Represent Postulated Flaws

		Nozzles	
			74
			75
			76
			77
		1	78
Geometry Inputs			
R1 (RVCH inner radius to base metal)	inches		
R2 (R1 + J-groove depth + crack growth)	inches		
dbore (nozzle bore diameter)	inches		
Cx (x distance from RVCH CL to Nozzle CL)	inches		
Cy (y distance from RVCH CL to Nozzle CL)	inches		
Rh = (Cx^2+Cy^2)^0.5	inches		
L1 (distance from nozzle CL to cut radius)	inches		
L2 (distance from nozzle CL to cut radius)	inches		
Calculate Area, A2 (Uphill Weld Area Removed)			
xmin = Rh-L1	inches		
xmax = Rh-dbore/2	inches		
A2	square inches		
Calculate Area, A3 (Downhill Weld Area Removed)			
xmin = Rh+dbore/2	inches		
xmax = Rh+L2	inches		
A3	square inches		
Calculate total weld cross sectional area removed in model			
A2+A3	square inches		

For the outermost penetration the initial flaw areas are measured from the ANSYS workbench model to be [ ] in^2 on the uphill side and [ ] on the downhill side (see Figure 6-8). For the center penetration the initial flaw area on both the uphill and downhill side is conservatively estimated by taking rectangle bounding the J-groove and butter (Reference [12]).

[ ]

The area with crack growth is estimated by taking the square root of the area, adding a rounded up crack growth of [ ] (see Table 6-1 and Table 6-2), and squaring the result as illustrated schematically in Figure 6-9. The results of the calculation are shown in Table 6-6.

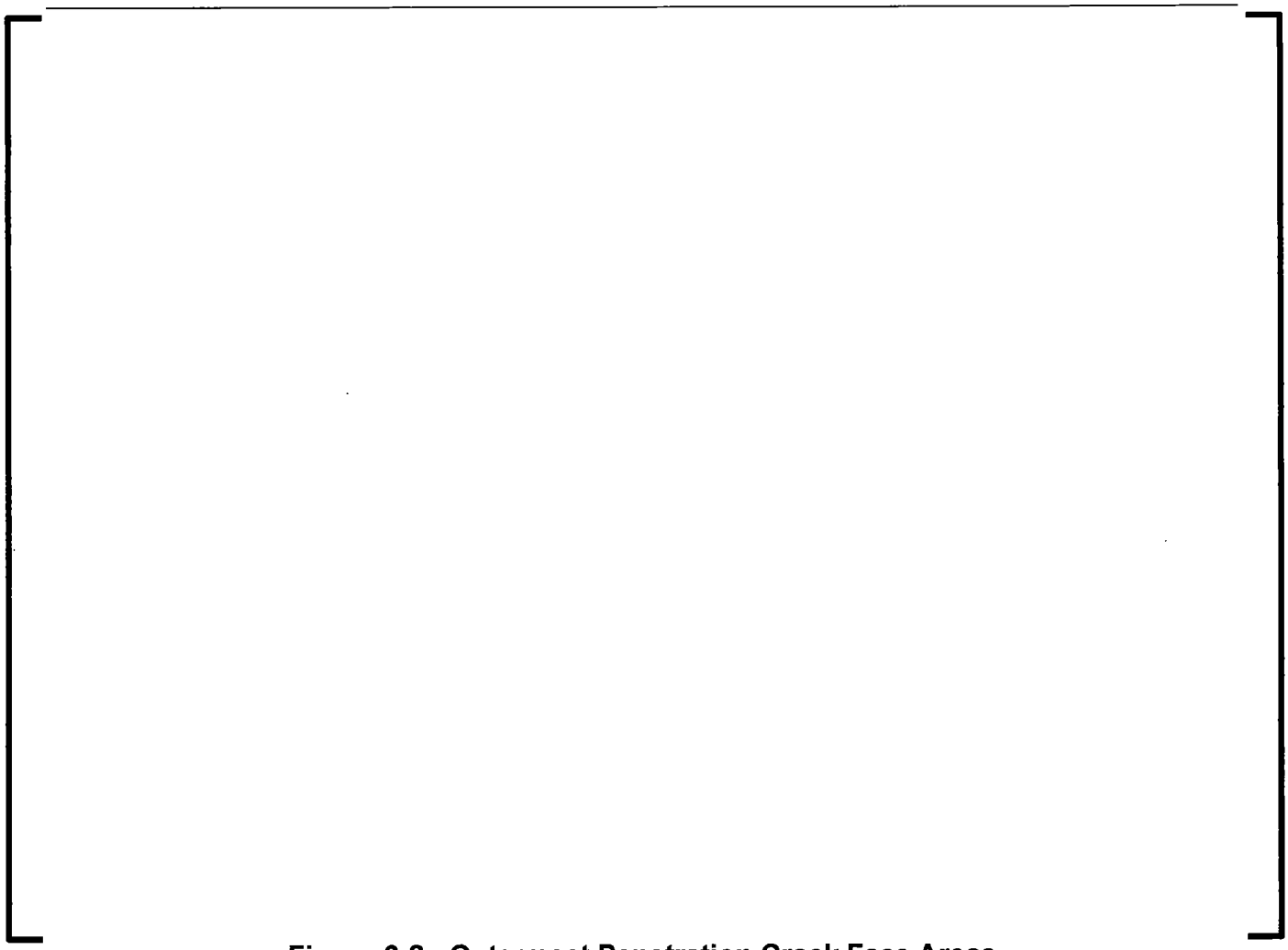

Figure 6-8: Outermost Penetration Crack Face Areas

[

]

Figure 6-9: Crack Growth Area Calculation

Table 6-6: Flaw Area Comparison

Nozzle		Center Nozzle	Outermost Nozzle
Uphill Weld Area	in^2	[ ]	[ ]
Downhill Weld Area	in^2	[ ]	[ ]
Max Crack Growth	inches	[ ]	[ ]
Uphill Weld Area with Max Crack Growth	in^2	[ ]	[ ]
Downhill Weld Area with Max Crack Growth	in^2	[ ]	[ ]
Uphill Area Removed, A2	in^2	[ ]	[ ]
Downhill Area Removed, A3	in^2	[ ]	[ ]
Uphill Area Removed - Uphill Area with Max CG	in^2	[ ]	[ ]
Downhill Area Removed - Downhill Area with Max CG	in^2	[ ]	[ ]

As shown above in Table 6-6 the areas removed from the ANSYS model (A2 and A3) exceeds the area including crack growth in all cases; therefore, sufficient area has been removed in the Limit Load model to account for the area of the flaw and crack growth.

Since sufficient area has been removed and the limit pressure exceeded 150% of the Design Pressure, the primary stress criteria in items 3.1(c) and 3.2(a)(3) of Code Case N-749 (Reference [3]) are satisfied.

7.0 CONCLUSIONS

A fatigue crack growth and fracture mechanics evaluation of the worst-case flaws in the as-left J-groove weld and buttering at the worst-case penetration location has been performed. Based on a combination of linear elastic and elastic-plastic fracture mechanics the postulated flaws are shown to be acceptable for the remaining life utilizing the safety factors in Table 1-1, and the lower bound J-R Curve from Regulatory Guide 1.161.

Limitation: The minimum metal temperature for performing a Hydrostatic test at any time after an IDTB repair has been made is [ ]

8.0 REFERENCES

1. AREVA Document 08-9232121-001, "Byron Units 1 and 2, and Braidwood Units 1 and 2, RVCH Nozzle Penetration Modification."
2. ASME Boiler and Pressure Vessel Code, Section XI, "Rules for Inservice Inspection of Nuclear Power Plant Components", 2001 Edition including Addenda through 2003.
3. Cases of the ASME Boiler and Pressure Vessel Code, Case N-749, "Alternative Acceptance Criteria for Flaws in Ferritic Steel Components Operating in the Upper Shelf Temperature Range," Section XI, Division I.
4. Letter, Balwant K. Singal (NRC) to Randall K. Edington (APS), "Palo Verde Nuclear Generating Station, Unit 3- Request for Additional Information RE: Relief Request 52, Alternative to ASME Code, Section XI Requirements for Flaw Evaluation, Flaw Characterization, and Successive Examinations (TAC NO. MF4169)," NRC ADAMS Accession Number ML14330A510, December 4, 2014.
5. T.L. Anderson, "Fracture Mechanics – Fundamentals and Applications", CRC Press, 1991.
6. AREVA Document 38-2201373-001, "Byron Units 1&2 and Braidwood Units 1&2 Proprietary Information."
7. AREVA Drawing 02-185313E-00, "Closure Head Assembly."
8. AREVA Drawing 02-185314E-00, "Closure Head Sub-Assembly Sheet 1."
9. AREVA Drawing 02-185344E-00, "Closure Head Assembly."
10. AREVA Drawing 02-185345E-00, "Closure Head Sub-Assembly Sheet 1."
11. AREVA Drawing 02-184573E-04, "Closure Head Assembly."
12. AREVA Drawing 02-184574E-06, "Closure Head Sub-Assembly Sheet 1."
13. AREVA Drawing 02-185282E-00, "Closure Head Assembly."
14. AREVA Drawing 02-185283E-01, "Closure Head Sub-Assembly Sheet 1."
15. AREVA Drawing 02-9232823E-001, "Byron Units 1 and 2 / Braidwood Units 1 and 2 CRDM, SPARE & RVLIS Penetration Modification."
16. AREVA Drawing 02-9232824E-001, "Byron Units 1 and 2 / Braidwood Units 1 and 2 Thermocouple Column Penetration Modification."
17. ASME Boiler and Pressure Vessel Code, Section III, "Nuclear Power Plant Components," Division 1, 1971 Edition including Addenda through Summer 1973
18. AREVA Document 51-9234885-000, "Exelon Byron and Braidwood RVCH Original Material and Fabrication Review."
19. ASTM E185-10, "Standard Practice for Design of Surveillance Programs for Light-Water Moderated Nuclear Power Reactor Vessels."
20. Regulatory Guide 1.161, "Evaluation of Reactor Pressure Vessels with Charpy Upper-Shelf Energy Less than 50 ft-lb", June 1995.
21. AREVA Document 32-9233779-000, "Weld Residual Stress Analysis of Byron 1 & 2, and Braidwood 1 & 2 RVCH Nozzle/Penetration Repair"
22. AREVA Document 32-9233803-001, "ASME Section III Analysis of Byron/Braidwood RVCH Nozzle and Penetration Modification"
23. ANSYS Finite Element Computer Code, Version 14.5, ANSYS Inc., Canonsburg, PA.
24. ASME Boiler and Pressure Vessel Code, Section III, "Rules for Construction of Nuclear Facility Components", Division 1, 2001 Edition including Addenda through 2003.
25. AREVA Drawing 02-185318E-01, "Closure Head Attachments."
26. Hill, R., "The Mathematical Theory of Plasticity," Oxford University Press, 1950.
27. Avalone, E.A., Baumeister, T., Sadegh, A.M., (Eds.) "Marks' Standard Handbook for Mechanical Engineers," Eleventh Edition, McGraw Hill.

28. ASME Boiler and Pressure Vessel Code, Section XI, "Rules for Inservice Inspection of Nuclear Power Plant Components", 2007 Edition including Addenda through 2008.
29. Federal Register, Volume 81, Page 10787 (81 FR 10787), Wednesday March 2, 2016, Proposed Rules.

APPENDIX A: UPHILL SIDE FLAW EVALUATIONS

This appendix presents the fatigue crack growth and flaw evaluations for the uphill side flaw.

Table A-1: SIFs for Uphill Side – Welding Residual Stress

[

]

Table A-2: SIFs for Uphill Side – Design Condition

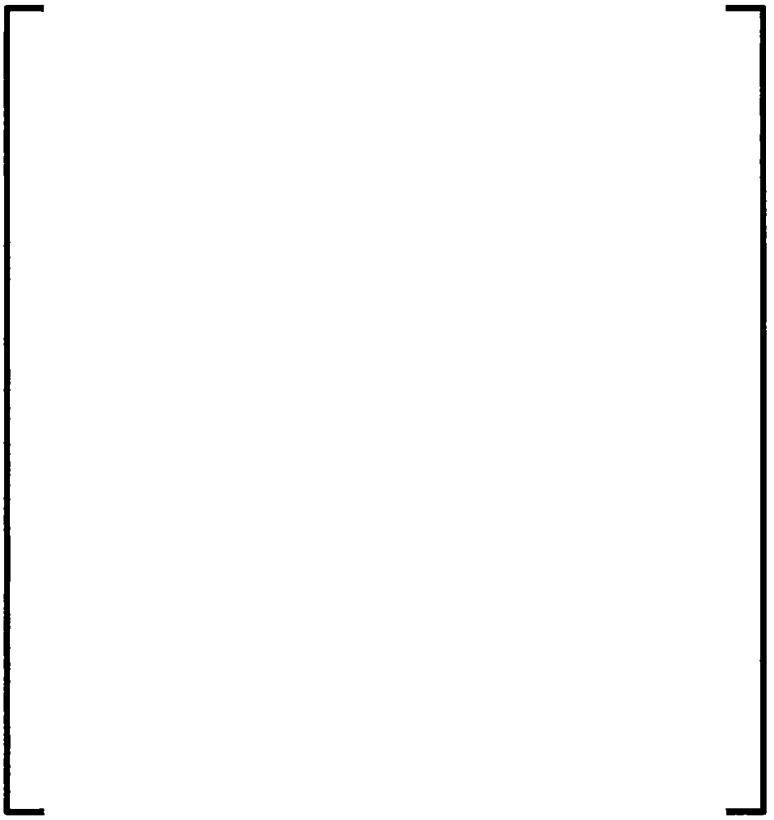

Table A-3: SIFs for Uphill Side – [ ]

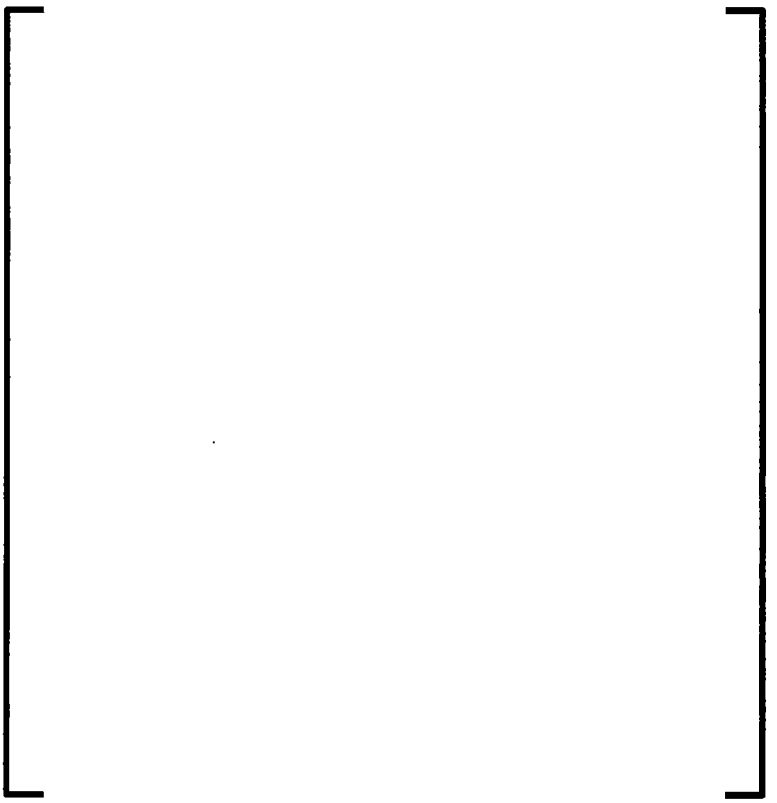

Table A-4: SIFs for Uphill Side – [ ]

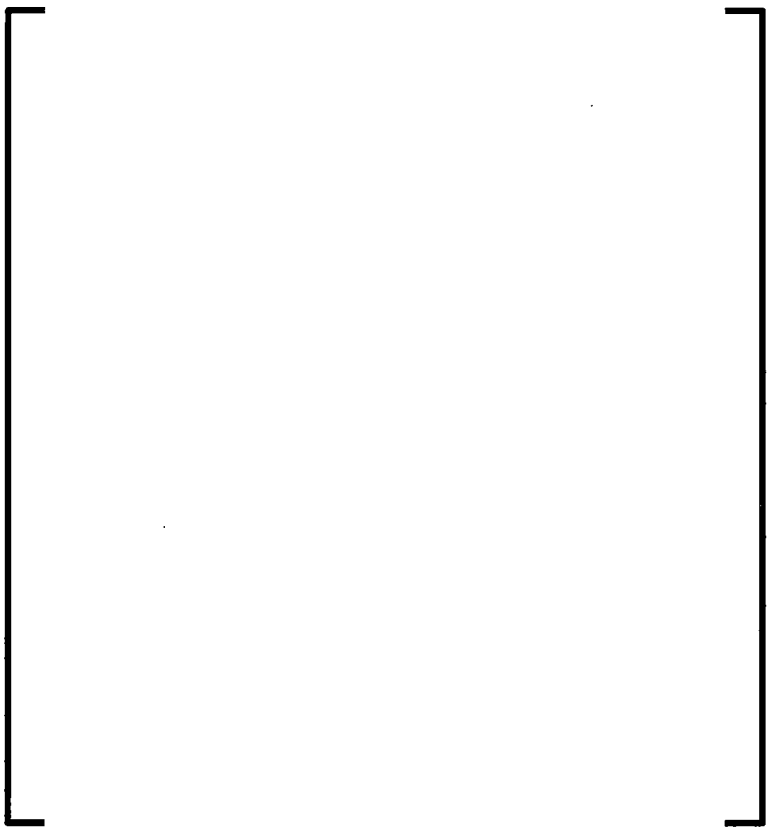

Table A-5: SIFs for Uphill Side – [ ]

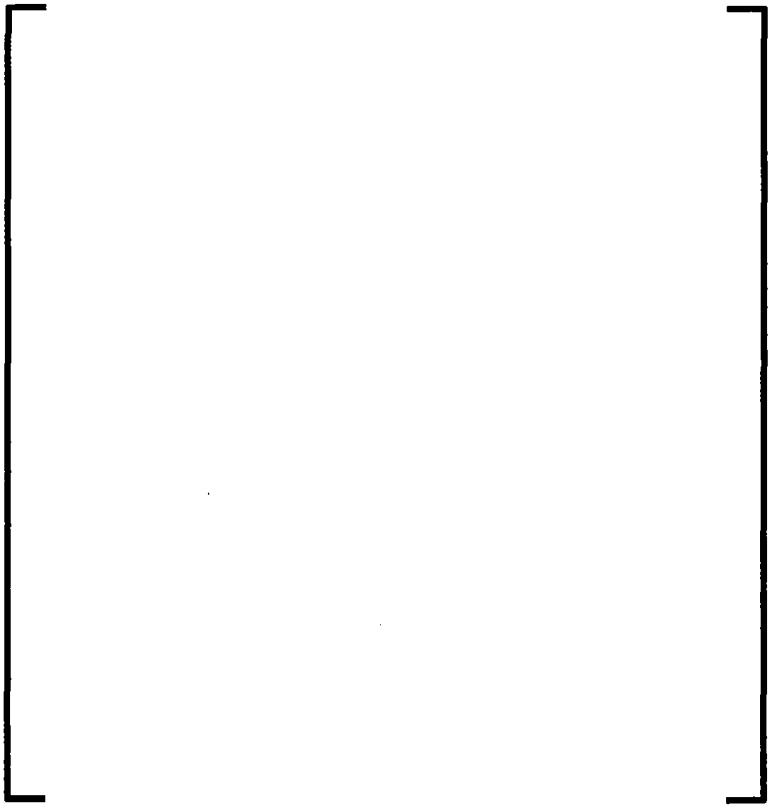

Table A-6: SIFs for Uphill Side – [ ]

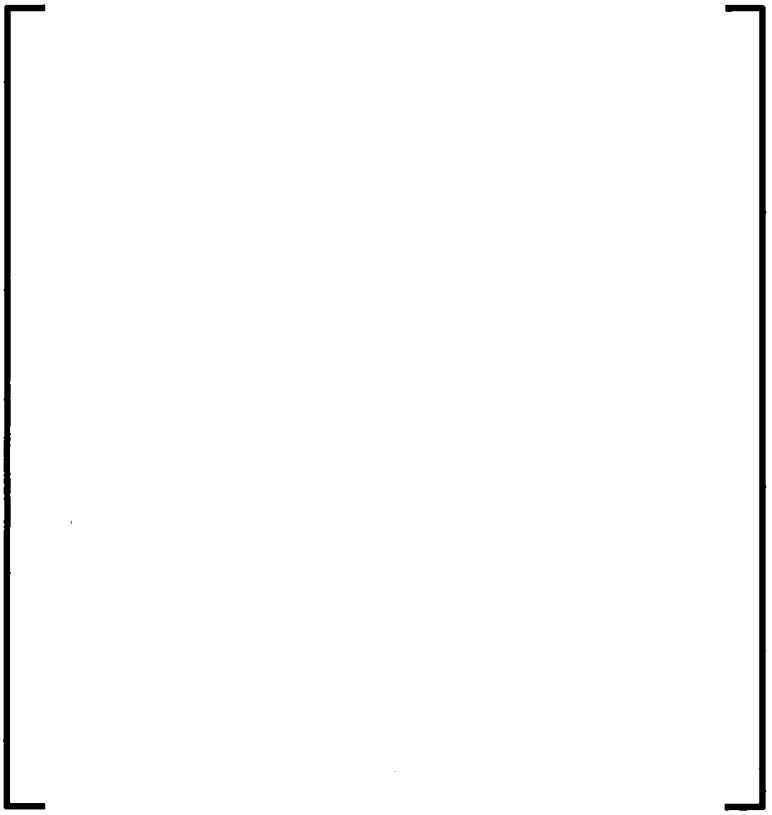

Table A-7: Fatigue Crack Growth for [ ] (Uphill)

Table A-8: Fatigue Crack Growth for [ ] (Uphill)

Table A-9: Fatigue Crack Growth for [ ] (Uphill)

Table A-10: Fatigue Crack Growth for [ ] (Uphill)

Table A-11: Fatigue Crack Growth [ ] (Uphill)

Table A-12: Fatigue Crack Growth for [ ] (Uphill)

Table A-13: Fatigue Crack Growth for [ ] (Uphill)

Table A-14: Fatigue Crack Growth for [ ] (Uphill)

[

]

Table A-15: Fatigue Crack Growth for [ ] (Uphill)

Table A-16: Fatigue Crack Growth for [ ] (Uphill)

Table A-17: Fatigue Crack Growth for [ ] (Uphill)

Table A-18: Fatigue Crack Growth for [ ] (Uphill)

Table A-19: Fatigue Crack Growth for [ ] (Uphill)

Table A-20: Fatigue Crack Growth for [ ] (Uphill)

Table A-21: Fatigue Crack Growth for [ ] (Uphill)

Table A-22: EPFM Evaluation for [ ] (Uphill)

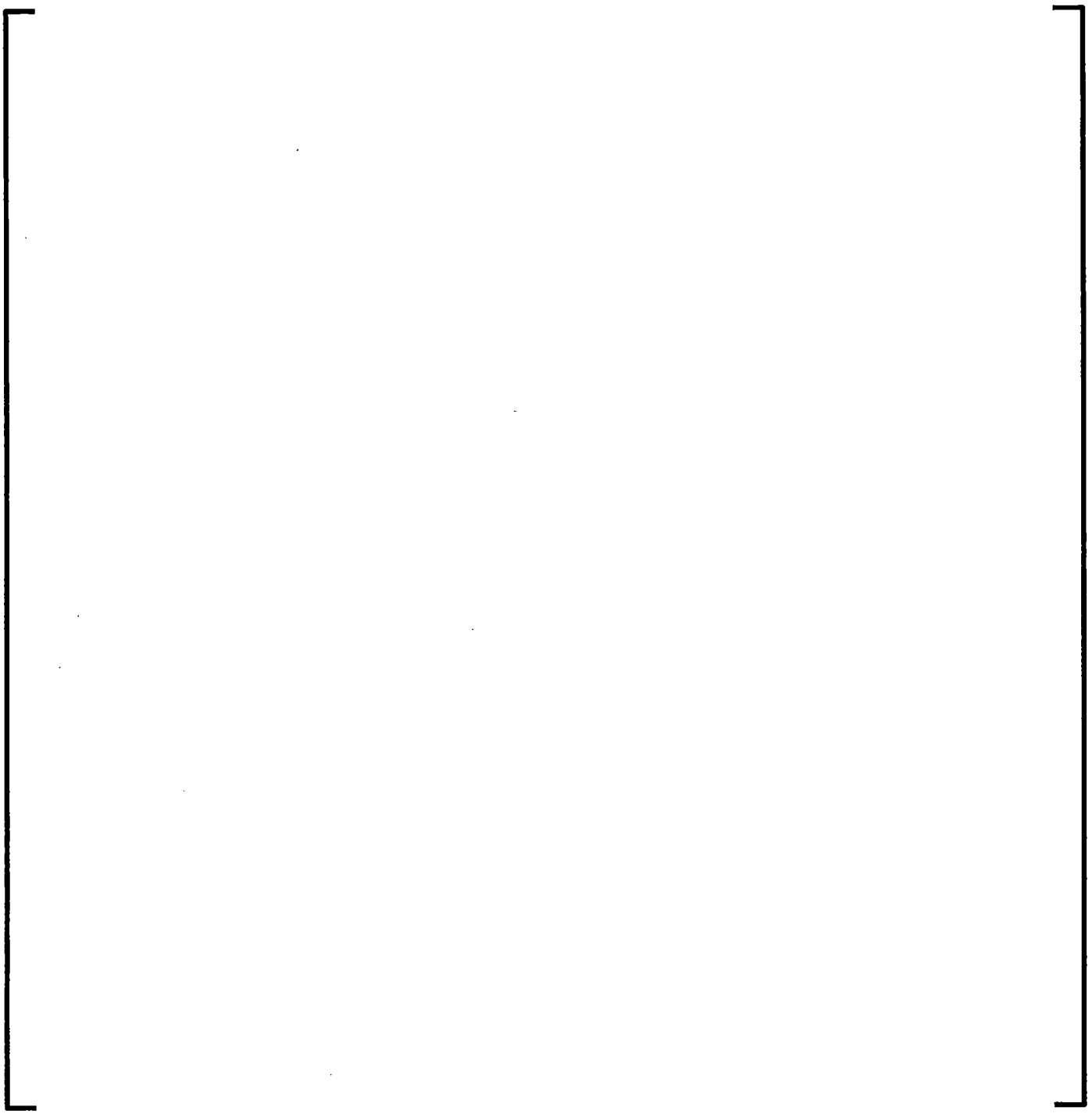

Figure A-1: J-T Diagram for [ ] (Uphill)

APPENDIX B: DOWNHILL SIDE FLAW EVALUATIONS

This appendix presents the fatigue crack growth and flaw evaluations for the downhill side flaw.

Table B-1: SIFs for Downhill Side – Welding Residual Stress

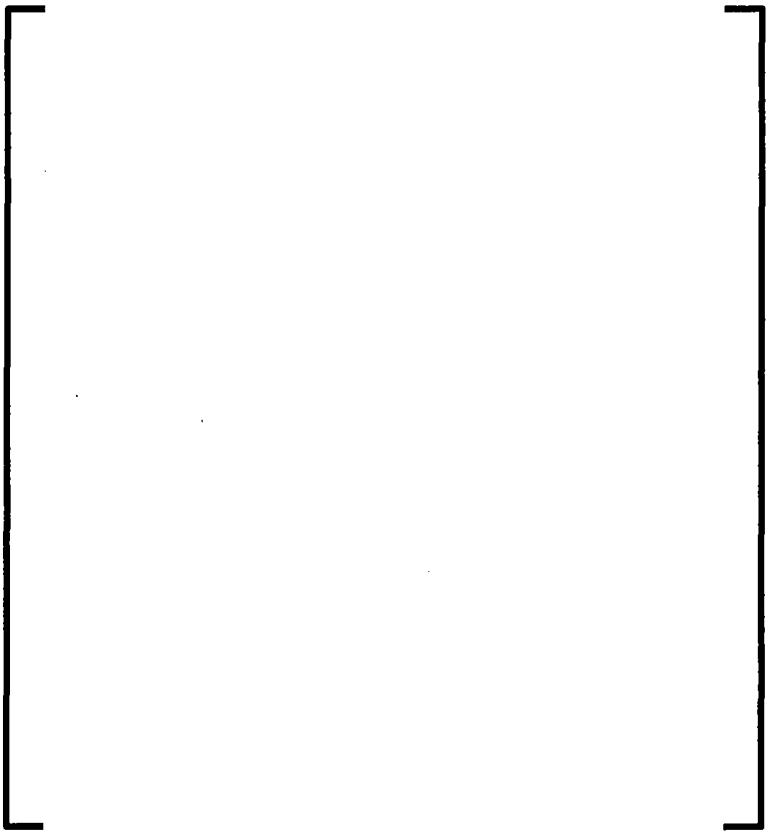

Table B-2: SIFs for Downhill Side – Design Condition

[

]

Table B-3: SIFs for Downhill Side – [ ]

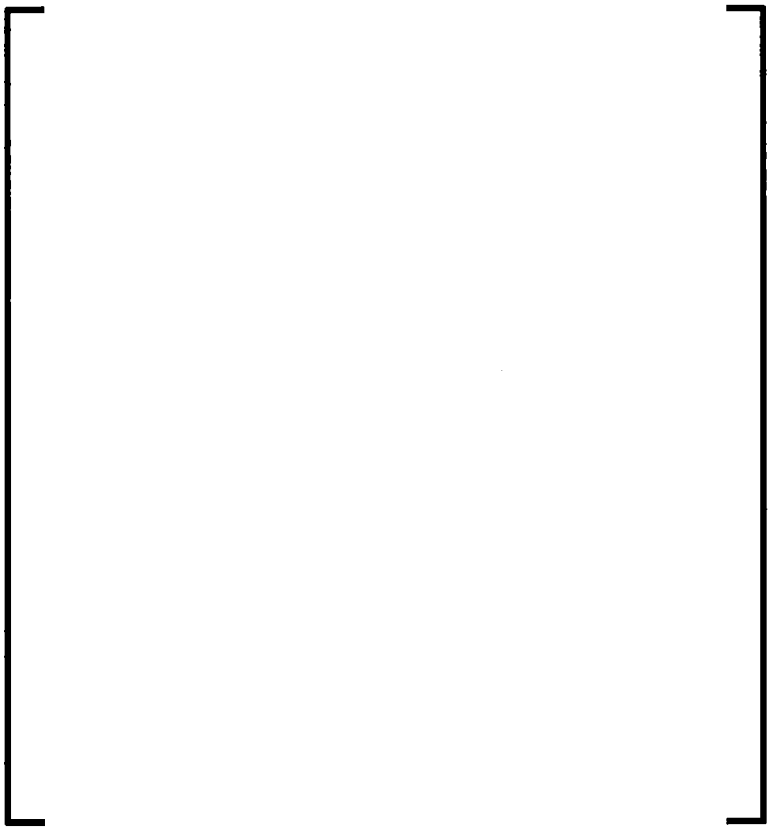

Table B-4: SIFs for Downhill Side – [ ]

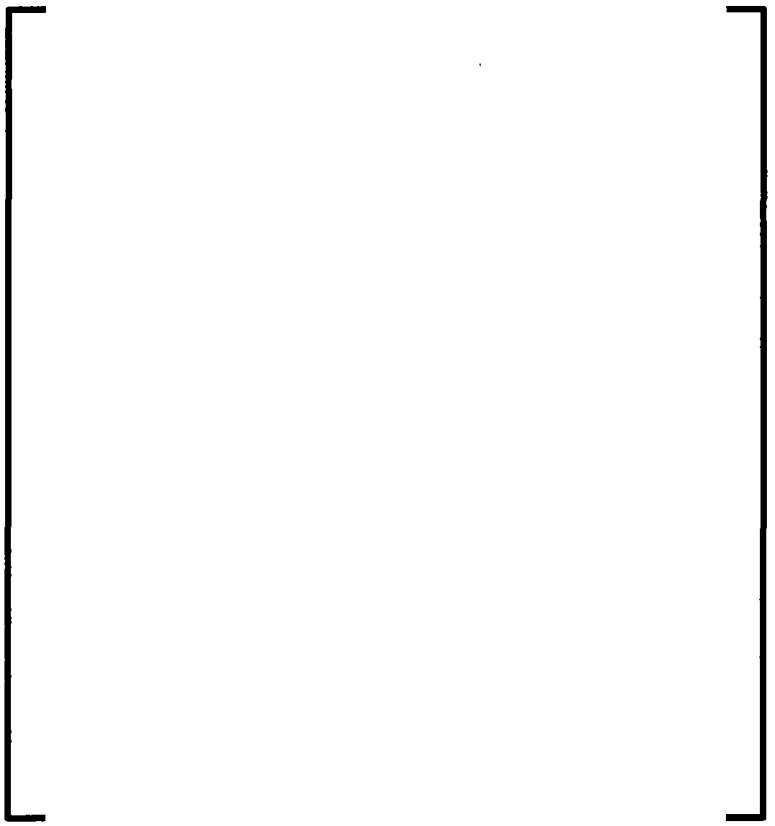

Table B-5: SIFs for Downhill Side – [ ]

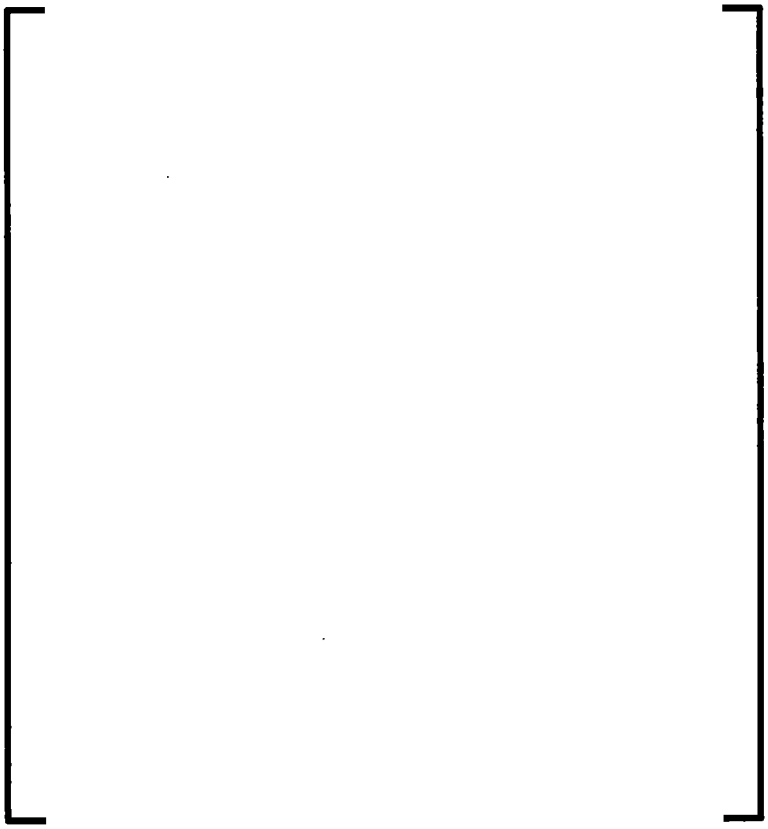

Table B-6: SIFs for Downhill Side – [ ]

[

]

Table B-7: Fatigue Crack Growth for [ ] (Downhill)

[

]

Table B-8: Fatigue Crack Growth for [ ] (Downhill)

Table B-9: Fatigue Crack Growth for [ ] (Downhill)

Table B-10: Fatigue Crack Growth for [ ] (Downhill)

[

]

Table B-11: Fatigue Crack Growth for [ ] (Downhill)

Table B-12: Fatigue Crack Growth for [ ] (Downhill)

Table B-13: Fatigue Crack Growth for [ ] (Downhill)

Table B-14: Fatigue Crack Growth for [ ] (Downhill)

Table B-15: Fatigue Crack Growth for [ ] (Downhill)

Table B-16: Fatigue Crack Growth for [ ] (Downhill)

Table B-17: Fatigue Crack Growth for [ ] (Downhill)

[

]

Table B-18: Fatigue Crack Growth for [ ] (Downhill)

[

]

Table B-19: Fatigue Crack Growth for [ ] (Downhill)

Table B-20: Fatigue Crack Growth for [ ] (Downhill)

Table B-21: Fatigue Crack Growth for [ ] (Downhill)

Table B-22: EPFM Evaluation for [ ] (Downhill)

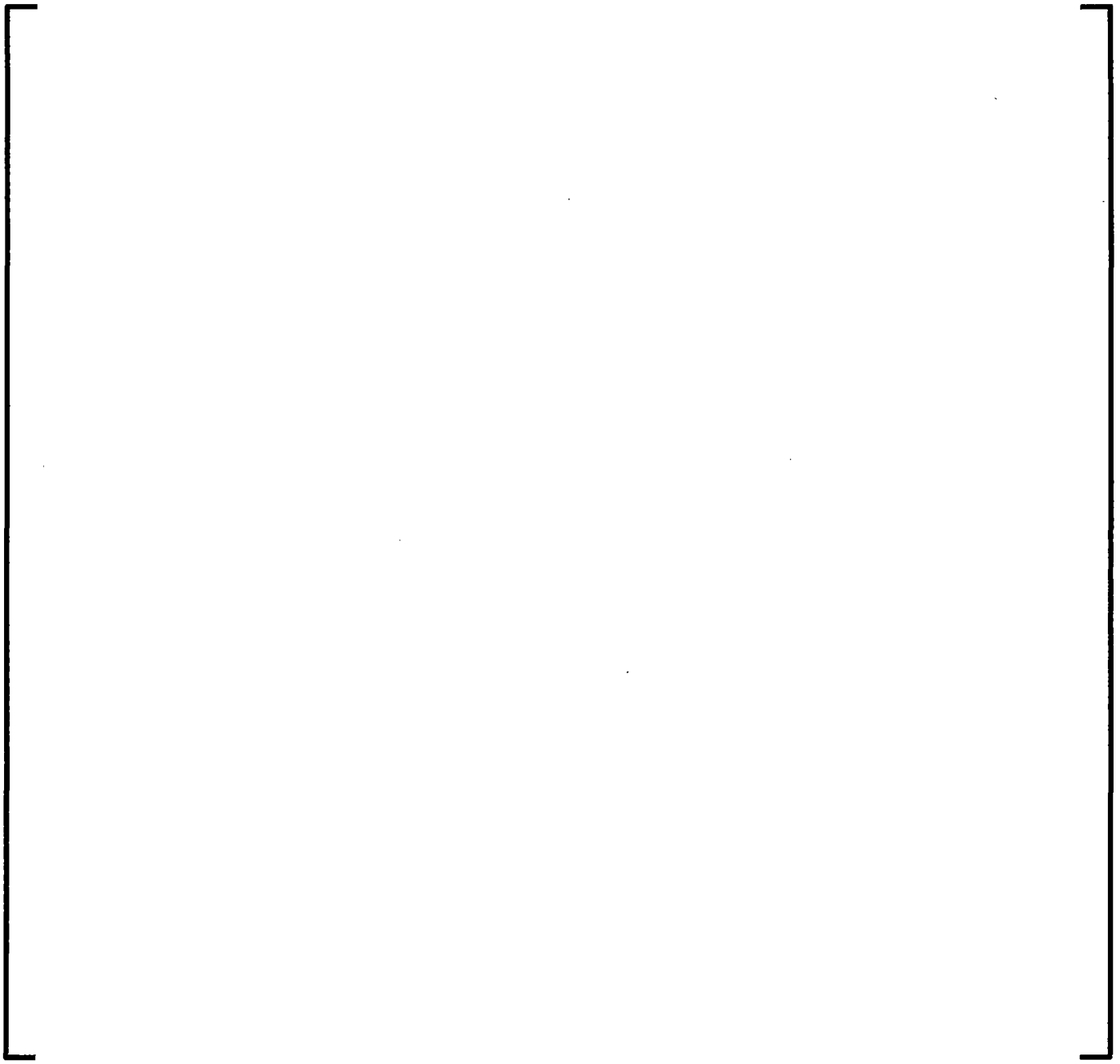

Figure B-1: J-T Diagram for [ ] (Downhill)

APPENDIX C: EVALUATION OF THE [ ] TRANSIENT

C.1 Purpose

The purpose of this appendix is to evaluate the [ ] defined in Reference [6] (TODI BYR-16-023).

C.2 Evaluation

Transient stresses for the [ ] were developed in Reference [22] (file [ ]), and applied to the explicit flaw models as described in the main body of this report to determine stress intensity factors. The computer files for this run are documented in Table 5-2. The resulting minimum and maximum stress intensity factors for this transient from the "*.KI" files (Table 5-2) are listed in Table C-1 for the uphill side and Table C-2 for the downhill side.

Table C-1: SIFs for Uphill Side - [ ]

Table C-2: SIFs for Downhill Side - [ ]

The [ ] has [ ] design cycles and is an [ ] condition per Reference [6] (TODI BYR-16-023). From Table C-1 at position 17 on the uphill side [ ], and from Table C-2 at position 17 for the downhill side [ ]. Based on these stress intensity factor ranges, and comparison with the crack growth results presented in Appendix A and Appendix B, [ ] cycles of [ ] would result in crack growth of only a few mils; this growth is negligible relative to the large postulated flaw sizes and the existing calculated crack growth. Therefore, the fatigue crack growth analysis need not consider the [ ], and final flaw sizes calculated in the main body (see Table 6-1 and Table 6-2) remain applicable with the inclusion of the [ ] transient.

The LEFM evaluations described in Section 6.3 are performed for the uphill position 17 and downhill position 17 in spreadsheets "LEFM_FCG_uh_EFT.xlsm" and "LEFM_FCG_dh_EFT.xlsm" (see Table 5-2). The results are summarized in Table C-3 and Table C-4. Similar to the other transient LEFM analyses in Section 6.3, the LEFM acceptance criteria are not satisfied, however the temperature is in the upper shelf range (> T_c), and therefore EPFM methodology is applicable.

Table C-3: Uphill Position 17 [ ] LEFM Results

[

]

Table C-4: Downhill Position 17 [ ] LEFM Results

[

]

The EPFM analyses are perfomed in the spreadsheets "EPFM-RG1161_uh_EFT.xlsm" and "EPFM-RG1161_dh_EFT.xlsm" (see Table 5-2) following the methodology described in the main body of the report. The results are summarized in Table C-5 and Table C-6 for the uphill and downhill sides, respectively. In both cases, considering the higher safety factors provided in Section 3.1 of Reference [3], the applied J-Integral is less than the material J-Integral at a ductile crack extension of 0.1 in. Although not required with use of the safety factors from Section 3.1 of Reference [3] for the applied J-Integral check, the stability check is performed for completeness and is also satisfied.

Table C-5: Uphill Position 17 [ ] EPFM Results

[

]

Table C-6: Downhill Position 17 [ ] EPFM Results

[

]

C.3 Conclusion

Based on the evaluation above, the [ ] transient satisfies the acceptance criteria of Code Case N-749 (Reference [3]) for the remaining life of the postulated flaws.